



# Synchronization and firing patterns of coupled Rulkov neuronal map

Sarbendu Rakshit · Arnob Ray · Bidesh K. Bera · Dibakar Ghosh

Received: 2 January 2018 / Accepted: 27 May 2018  
© Springer Science+Business Media B.V., part of Springer Nature 2018

**Abstract** In this paper, we investigate stabilization, neuronal synchrony and different neuronal dynamics in two coupled neuronal Rulkov map in the presence of both inner linking function and chemical synaptic interactions. Based on linear stability analysis, conditions for stability of the fixed point for this coupled system are derived. Through master stability function approach, the local stability of complete synchronization is studied by calculating the transverse Lyapunov exponents of error system and using basin stability measure, we quantify the global stability of synchronization. More interestingly, different transitions of the neural spiking–bursting synchronous patterns are found for appropriately chosen interaction strengths. We interrogate the effect of time delay in the interaction function, and surprisingly, we observe that delay time can induce the mixed type of behavior to achieve the complete neuronal synchronous state. The presence of time delay solely in inner linking coupling is favorable for synchronization, while the presence of delay in both the interactions, the synchronization enhanced up to a certain threshold of delay time and beyond that it demolish the neural synchrony. The neuronal synchronization is also studied in coupled system with stochastic on–off interaction, exemplify by, in neural network neurons interact through sending short pulses, called spike. The different types of neuron dynamics

are observed when a resting neuron is interacting with a bursting neuron under the proposed coupling configuration. Finally, the autaptic connection induces and enhances the complete synchronization behavior.

**Keywords** Chaotic Rulkov neural map · Inner linking function · Firing–resting pattern · Neural synchronization · Master stability function · Basin stability · Time-delayed interaction · Blinking interaction · Autapse

## 1 Introduction

Understanding the inter-neuronal communication between neurons through synapses is a challenging issue due to the presence of large number of neurons and thousand times more synapses in human brain [1]. The brain function relies on the communications between the neurons which take places through two different types of synapses, namely chemical and electrical synapses. These two modalities synapses are mainly functional connections in which the information passes from one neuron to other neurons. Through chemical synapse, information passes chemically between two neurons. In probabilistic manner, pre-synaptic neuron releases neurotransmitter molecules (acetylcholine, gamma-aminobutyric acid, dopamine, serotonin, etc.) into the synaptic cleft that is adjacent to another neuronal cell. These molecules then bind by the post-synaptic receptors side of that synaptic cleft. The

S. Rakshit · A. Ray · B. K. Bera · D. Ghosh (✉)  
Physics and Applied Mathematics Unit, Indian Statistical Institute, 203 B. T. Road, Kolkata 700108, India  
e-mail: dibakar@isical.ac.in

chemical and electrical synapses both can coexist in most of the nervous system and operate independently [2]. Recently, Sun et al. [3] investigate complete synchrony in coupled Rulkov neuronal network by designing a specific inner linking function, which is different from the usual electrical and chemical synaptic interactions. So the study on neuronal synchrony together with other collective dynamics in coupled neuron in the presence of both inner linking and chemical synaptic communications is still deserved a special attention.

There are several highly rich collective dynamics appear due to the neuronal interactions, among them synchronization is the most prominent collective features in the field of neuroscience, which proposed as one of the mechanisms to transmit and to code information in brain [4,5]. In many neural systems, such as mammalian visual cortex, human thalamocortical area, and the stomatogastric ganglion of the spiny lobster, complete synchronization has been observed experimentally [6–8], also phase synchronization in human cardiorespiratory system [9]. There are different types of brain disorder diseases like Parkinson's, Alzheimer's, epilepsy and schizophrenia which are associated to the abnormal pattern of synchronization [10] in brain. Thus, the neuronal synchrony in the field of neuroscience is a fundamental issue.

Time delay interactions are omnipresent in real life systems and unavoidable due to the finite transmission speeds in many physical, biological and social systems, where the future evolution not only depends on present state but also depends on the state of the system some time interval before. For the inter-cellular communication between the pair of neurons in the brain, time delay is spatially distributed due to different distances and finite information transmission speeds. Particularly, for the case slow inhibitory synapse, time lapses appear by both dendrite and synaptic processing [11–13]. The stability, bifurcation and synchronization scenarios have studied in Ref. [14] analytically and numerically by taking four neuronal subnetwork with time-delayed coupling and they observed that the node dependency in the subnetwork plays a key role in the network characteristic. The controlling of neural synchronization was investigated in recurrent neural networks [15] in the presence of discrete and distributed delay coupling function. Very recently, under the field coupling, the collective behavior of the neural network was studied by Xu et al. [16]. Song et al. [17,18] dis-

cussed the generation and transition among the different types of bursting dynamics of the neural systems in the presence of time-delayed coupling. Using distributed delay in the nonlinear lattice of cellular neural networks, the exponential stability analysis of traveling waves is investigated in Ref. [19]. Time delay has been analyzed separately in both electrical and chemical types of interactions [20–24]. So, the influence of time delay in the neuronal synchrony is very important and has received significant attention. Most of the previous researches have been done in the study of different patterns of synchronization in coupled neuronal systems [25–33] by considering the instantaneous coupling function [34,35] and did not reveal the effect of time delay in the interaction, while the time delay interaction is ubiquitous in inter-cellular communication in brain which is happened through simultaneous presence of the both chemical and electrical synapses. In the inter-neuronal communication among the large number of neurons in the networks, the neurons are mostly organized in a subnetwork and the interaction between the sub-ensembles takes place only sporadically. Such type of interaction is the mimic of blinking or on-off type of interaction, and here we study the stochastic blinking effect in the neural synchrony. By applying impulse control technique and constructing the Lyapunov functions, the global stability analysis of stochastic neural network has been studied in the presence of time-varying delay [36].

One of the most fascinating emerging behavior appears due to interaction between the firing and resting dynamics which are strongly linked up with the several neuronal processes. The feasible biological applications of such processes are usually shown in mammalian circadian clocks, which consist of both active and inactive clock cells [37] and neuro-degenerative diseases, like Alzheimer's disease, which are characterized by progressive neuron fallout and also the connections between neurons are time delayed [38]. When these two types of neurons are interacted with each other, the intrinsic dynamics of each neuron changes depending on the coupling strength and consequently converges to either synchronous firing or resting processes. An another part of synaptic connection is an autapse [39] which exist in the neuronal network and plays a important role in the inter-neuronal communication. This type of connection was observed in 80% [40] of the investigated neurons, referred as a synaptic connection from a neuron to itself, and it formed by the

axon of a neuron on its own dendrite. Autapse induced synchronization [41] and wave propagation between the coupled chain of neural networks were studied in Refs. [42,43].

The classical pathway to study the stability of the synchronization in complex dynamical systems is investigated by master stability function (MSF) approach [44]. In the terminology of MSF, the master stability equation (MSE) is a set of linear systems obtained by linearizing the dynamical network near synchronization manifold and then convert the network into the transverse direction of the synchronization manifold. For the occurrence of synchronization, the negative maximum Lyapunov exponent of these MSE are a necessary condition for small perturbation, but not sufficient in the case of non-small random perturbation from synchronization manifold. To get rid from such local concept, Menck et al. [45] proposed the notion of basin stability (BS) based on the volume of the basin of attraction instead the traditional linearized based approach. BS is the nonlinear, non-local concept and a robust gadget for multi-stable system. In the field of neuroscience, multi-stable features are present in the different collective behavior which are emerged due to the interaction of several neuronal oscillators. To quantify the various collective behaviors such as synchronization and steady state, basin stability [46–48] approach is one of the pioneer measurements, nowadays.

Motivated by the above facts, we systematically study the synchronization and steady state in the presence of both inner linking and chemical synaptic interactions in coupled neurons. Our aim is to analyze the complete neuronal synchrony in two coupled neuronal Rulkov map with inner linking coupling function and chemical synapse using analytical and numerical approaches. To do this, we suitably design a general inner coupling function instead of electrical synaptic coupling function where a particular form of inner linking function also represents electrical synapse. The systematic representation of the interaction between the neurons is shown in Fig. 1. The main focus of our study of such coupled neurons is explored in the following way:

1. Through the linear stability analysis, we derive the stability conditions of the steady states of coupled systems and also the necessary conditions for neuronal synchrony derived analytically using MSF

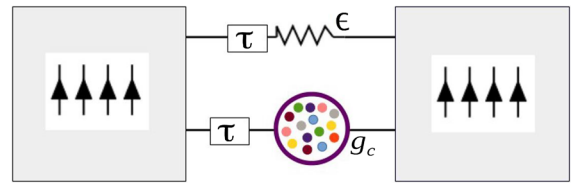


**Fig. 1** Schematic diagram of interaction between the two neurons with chemical synaptic and inner linking coupling. Here  $\epsilon$  and  $g_c$  are the coupling strengths of inner linking and chemical synaptic interactions, respectively, and  $\tau$  represents the transmission delay time

approach. Then, we quantify its global stability by BS measurement.

2. We investigate the effect of time delay in the inner linking and chemical synaptic coupling function in two coupled neurons. In this context, we find that time delay can significantly influence the critical threshold of inner coupling and chemical synaptic strength in which the coupled systems experiences the different synchronization patterns in a wide range of parameter space.
3. We study the stability of synchronous states using stochastically blinking interaction over time between the neurons. We clearly articulate the phenomena of enhancement of the complete neuronal synchrony of the coupled neuron under time delay and stochastic blinking interactions.
4. Under the influence of autaptic time delay, the neuronal synchrony is studied where the coupled neuron is in desynchronize state in the absence of autapse. The phenomena of neuronal synchrony are analyzed by changing the synaptic coupling delay and autaptic delay time in a wide range.
5. Finally, we investigate the dynamics of two coupled neurons where one is in firing mode and another is in silence state and how does the parameter mismatched promotes the different types of bursting and spiking behaviors in the silence neuron?

The remaining parts of this paper are organized as follows. The next Sect. 2 is devoted for the study of coupled Rulkov map in the presence of inner coupling and chemical synapses. In Sect. 3, we derive the analytical conditions for steady states which excellently match with our obtained numerical results. Using master stability function and basin stability approach, the local and global stability of synchronization state are analyzed in Sect. 4. The effect of time delay in the synaptic function is discussed in Sect. 5, and the synchronous

states with on–off coupling is provided in Sect. 5.2. The autaptic time delay induce synchrony is discussed in Sect. 5.3. Then, we study the synchronization and steady state dynamics of coupled systems while one neuron is in resting or silence mode and other neuron is in firing pattern, and the results are discussed in Sect. 6. Finally, we summarize our findings in Sect. 7.

## 2 Coupled Rulkov map

To study the different collective dynamical states of coupled neuronal systems, we consider computationally most expedient two-dimensional nonlinear Rulkov map [49, 50]. Depending on the different system parameter values, this neuronal map is capable of reproducing various types of firing patterns including spiking, bursting and silent state. The mathematical form of two coupled Rulkov map in the presence of chemical synapse and inner coupling function is represented by the set of equations

$$\begin{aligned} \mathbf{x}_1(n+1) &= f(\mathbf{x}_1(n), \mathbf{y}_1(n), \alpha_1) \\ &\quad + g_c(v_s - \mathbf{x}_1(n))\Gamma(\mathbf{x}_2(n)) \\ &\quad + \epsilon[f(\mathbf{x}_2(n), \mathbf{y}_2(n), \alpha_2) \\ &\quad - f(\mathbf{x}_1(n), \mathbf{y}_1(n), \alpha_1)], \\ \mathbf{y}_1(n+1) &= \mathbf{y}_1(n) - \eta(\mathbf{x}_1(n) - \sigma), \\ \mathbf{x}_2(n+1) &= f(\mathbf{x}_2(n), \mathbf{y}_2(n), \alpha_2) \\ &\quad + g_c(v_s - \mathbf{x}_2(n))\Gamma(\mathbf{x}_1(n)) \\ &\quad + \epsilon[f(\mathbf{x}_1(n), \mathbf{y}_1(n), \alpha_1) \\ &\quad - f(\mathbf{x}_2(n), \mathbf{y}_2(n), \alpha_2)], \\ \mathbf{y}_2(n+1) &= \mathbf{y}_2(n) - \eta(\mathbf{x}_2(n) - \sigma), \end{aligned} \quad (1)$$

where  $f(\mathbf{x}_i, \mathbf{y}_i, \alpha_i) = \frac{\alpha_i}{1 + \mathbf{x}_i^2} + \mathbf{y}_i$  for  $i = 1, 2$ . The parameter  $\sigma$  represents emulating the action of an external dc bias current given to the neuron, while  $\alpha_i$  is a control parameter which plays a vital role in producing the regime of different types of firing patterns like silence (resting), tonic spiking, regular and chaotic bursting, etc. Here the variable  $\mathbf{x}_i(n)$  exhibits fast dynamics and represents the trans-membrane potential of the  $i$ -th neuron at the discrete time step  $n$ , and  $\mathbf{y}_i(n)$  is a slow dynamical variable as long as  $\eta$  is small ( $0 < \eta \ll 1$ ) and conveys the variation of the ionic recovery currents. The chemical synaptic coupling function  $\Gamma(\mathbf{x}_i)$  is nonlinear and it is described by the sigmoidal input–

output function as  $\Gamma(\mathbf{x}) = \frac{1}{1+\exp[-k(\mathbf{x}-\Theta_s)]}$ , and the third term of Eq. (1)(first and third equation) represents the inner linking coupling function as  $f(x, y, \alpha)$ . In particular, if the inner linking coupling is a function of membrane potential variable  $x$  only, then the communication represents the electrical synaptic interaction. Previously, it was proved that if two Rulkov maps are communicated via electrical synapses solely, the two neurons can not attain synchrony [3] when the single neuron is in chaotic bursting state. For this reason, we consider the inner linking function as in general form. In an identical case,  $\alpha_1 = \alpha_2 = \alpha$ . The system parameters  $\alpha$  and  $\sigma$  determine whether the regime of the system is in rest, bursting or tonic spiking. The parameters  $g_c$  and  $\epsilon$  denote the chemical synaptic and inner coupling strengths, respectively, which summarize how the information is distributed through the interaction between the neurons.  $v_s$  is the synaptic reversal potential, for  $v_s > \mathbf{x}_i(n)$  the synaptic current has depolarizing effect, making the synapse excitatory, and if  $v_s < \mathbf{x}_i(n)$ , the synaptic current has hyper-polarizing effect, making the synapse inhibitory. The parameter  $k$  determines the slope of the sigmoidal function, and  $\Theta_s$  is the synaptic firing threshold. Complete synchronization (CS) is improbable for Rulkov model with electrical synapse, which is the difference between the membrane potential at the instantaneous time. Here, we model the inner linking function as the difference between the membrane potential of the isolate sub-system at the next time step. This inner coupling function is also adequate from the neural perspective. In the absence of inner linking function and chemical synaptic coupling strength, the map displays chaotic bursting behavior for  $4.0 < \alpha < 4.5$ , whereas for  $\alpha > 4.5$  chaotic spiking occurs. In our simulation, we fixed the parameter values at  $\alpha = 4.1$ ,  $\eta = 0.001$ ,  $\sigma = -1.6$ ,  $v_s = -1.4$ ,  $k = 50$ , and  $\Theta_s = -1.4$  [35].

## 3 Fixed point and linear stability analysis

Before we proceed into the spatiotemporal behavior of the coupled system, let us examine the local dynamics of the coupled system. The coupled system (1) has unique fixed point  $P$  and is given by  $(\sigma, \sigma - \frac{\alpha}{1+\sigma^2} + \frac{g_c(\sigma-v_s)}{1+\exp[-k(\sigma-\Theta_s)]}, \sigma, \sigma - \frac{\alpha}{1+\sigma^2} + \frac{g_c(\sigma-v_s)}{1+\exp[-k(\sigma-\Theta_s)]})$ . There is no effect of inner linking function strength  $\epsilon$  on the position of this fixed point.

Now we carry out a comprehensive qualitative analysis for stability of this fixed point. The Jacobian matrix of system (1) at the fixed point  $P$  is given by

$$J = \begin{bmatrix} -t(1-\epsilon) - ag_c & 1-\epsilon & -t\epsilon + bg_c & \epsilon \\ -\eta & 1 & 0 & 0 \\ -t\epsilon + bg_c & \epsilon & -t(1-\epsilon) - ag_c & 1-\epsilon \\ 0 & 0 & -\eta & 1 \end{bmatrix},$$

where  $t = \frac{2\alpha\sigma}{(1+\sigma^2)^2}$ ,  $a = \frac{1}{1+\exp[-k(\sigma-\Theta_s)]}$ ,  $b = \frac{-k(\sigma-v_s)\exp[-k(\sigma-\Theta_s)]}{(1+\exp[-k(\sigma-\Theta_s)])^2}$ . In the Jacobian matrix  $J$ , we have block matrices which simplifies the method of finding eigenvalues. The characteristic equation is a product of two quadratic polynomials and is given by

$$F_1(\lambda) F_2(\lambda) = 0, \quad (2)$$

where  $F_1(\lambda) = \lambda^2 - \lambda\{1-t(1-2\epsilon) - g_c(a+b)\} + \{(\eta-t)(1-2\epsilon) - g_c(a+b)\}$ , and  $F_2(\lambda) = \lambda^2 - \lambda\{1-g_c(a-b)-t\} + \{\eta-g_c(a-b)-t\}$ . If  $\Delta_{1,2}$  denote the discriminant of  $F_{1,2}(\lambda)$ , then we have  $\Delta_1 = [t(1-2\epsilon) + g_c(a+b) + 1]^2 - 4\eta(1-2\epsilon)$  and  $\Delta_2 = [g_c(a-b) + t + 1]^2 - 4\eta$ . The Jacobian matrix  $J$  has four eigenvalues, two of them depend on the sign of the discriminant  $\Delta_1$ , and another two depend on the sign of  $\Delta_2$ . Next we analyze the stability of the fixed point  $P$  of the system (1) according to the sign of the discriminant  $\Delta_1$  and  $\Delta_2$  of Eq. 2. We obtain four different cases as follows:

### Case I : $\Delta_1 \geq 0$ & $\Delta_2 \geq 0$

In this case, there exist four different real eigenvalues of  $J$ , obtain from  $F_1(\lambda) = 0$  and  $F_2(\lambda) = 0$  as follows:

$$\begin{aligned} \lambda_{1,1}^1 &= \frac{\{1-t(1-2\epsilon) - g_c(a+b)\} + \sqrt{\{t(1-2\epsilon) + g_c(a+b) + 1\}^2 - 4\eta(1-2\epsilon)}}{2}, \\ \lambda_{1,2}^1 &= \frac{\{1-t(1-2\epsilon) - g_c(a+b)\} - \sqrt{\{t(1-2\epsilon) + g_c(a+b) + 1\}^2 - 4\eta(1-2\epsilon)}}{2}, \\ \lambda_{2,1}^1 &= \frac{\{1-g_c(a-b)-t\} + \sqrt{\{g_c(a-b)+t+1\}^2 - 4\eta}}{2}, \\ \lambda_{2,2}^1 &= \frac{\{1-g_c(a-b)-t\} - \sqrt{\{g_c(a-b)+t+1\}^2 - 4\eta}}{2}. \end{aligned} \quad (3)$$

The fixed point  $P$  will be stable if all of the moduli of the eigenvalues of  $J$  are strictly less than one. For  $F_1(\lambda)$ , if  $|\lambda_{1,1}^1| < 1$  and  $|\lambda_{1,2}^1| < 1$ , then the following conditions are satisfied :

$$\left\{ \begin{array}{l} \Delta_1 \geq 0, \\ F_1(1) > 0, \\ F_1(-1) > 0, \\ -2 < \lambda_{1,1}^1 + \lambda_{1,2}^1 < 2, \\ -1 < \lambda_{1,1}^1 \cdot \lambda_{1,2}^1 < 1. \end{array} \right. \Rightarrow \left\{ \begin{array}{l} |g_c(a+b) + 1 + t(1-2\epsilon)| \geq 2\sqrt{\eta(1-2\epsilon)}, \\ \epsilon < \frac{1}{2}, \\ g_c(a+b) < 1 + \left(\frac{\eta}{2} - t\right)(1-2\epsilon), \\ -1 < g_c(a+b) + t(1-2\epsilon) < 3, \\ -1 < g_c(a+b) - (\eta - t)(1-2\epsilon) < 1. \end{array} \right. \quad (4)$$

And for  $F_2(\lambda)$ , if  $|\lambda_{2,1}^1| < 1$  and  $|\lambda_{2,2}^1| < 1$ , then we have :

$$\left\{ \begin{array}{l} \Delta_2 \geq 0, \\ F_2(1) > 0, \\ F_2(-1) > 0, \\ -2 < \lambda_{2,1}^1 + \lambda_{2,2}^1 < 2, \\ -1 < \lambda_{2,1}^1 \cdot \lambda_{2,2}^1 < 1. \end{array} \right. \Rightarrow \left\{ \begin{array}{l} |g_c(a-b) + t + 1| \geq 2\sqrt{\eta}, \\ \eta > 0, \\ 1 - g_c(a-b) - t + \frac{\eta}{2} > 0, \\ -1 < g_c(a-b) + t < 3, \\ -1 < g_c(a-b) - \eta + t < 1. \end{array} \right. \quad (5)$$

Combining all the inequalities from (4) to (5), we obtain the condition of stability of the fixed point  $P$  as:

- (a1)  $|g_c(a+b) + 1 + t(1-2\epsilon)| \geq 2\sqrt{\eta(1-2\epsilon)}$ ,
- (b1)  $|g_c(a-b) + t + 1| \geq 2\sqrt{\eta}$ ,
- (c1)  $(\eta - t)(1-2\epsilon) - 1 < g_c(a+b) < (\frac{\eta}{2} - t)(1-2\epsilon) + 1$ ,

$$\begin{aligned} (d_1) \quad & \eta - t - 1 < g_c(a - b) < \frac{\eta}{2} - t + 1, \\ (e_1) \quad & \eta > 0, \\ (f_1) \quad & \epsilon < \frac{1}{2}. \end{aligned}$$

**Case II :**  $\Delta_1 < 0$  &  $\Delta_2 < 0$

Under this condition there exist two pair of complex conjugate eigenvalues of the characteristic equation (2) as:

$$\begin{aligned} \lambda_{1,1}^2 &= \frac{\{1 - t(1 - 2\epsilon) - g_c(a + b)\} + i\sqrt{4\eta(1 - 2\epsilon) - \{t(1 - 2\epsilon) + g_c(a + b) + 1\}^2}}{2}, \\ \lambda_{1,2}^2 &= \frac{\{1 - t(1 - 2\epsilon) - g_c(a + b)\} - i\sqrt{4\eta(1 - 2\epsilon) - \{t(1 - 2\epsilon) + g_c(a + b) + 1\}^2}}{2}, \\ \lambda_{2,1}^2 &= \frac{\{1 - g_c(a - b) - t\} + i\sqrt{4\eta - \{g_c(a - b) + t + 1\}^2}}{2}, \\ \lambda_{2,2}^2 &= \frac{\{1 - g_c(a - b) - t\} - i\sqrt{4\eta - \{g_c(a - b) + t + 1\}^2}}{2}. \end{aligned} \quad (6)$$

The fixed point  $P$  will be stable if  $|\lambda_{i,j}^2| < 1$  for  $i, j \in \{1, 2\}$ . The moduli of these eigenvalues are easily calculated and found to be :  $|\lambda_{1,i}^2| = \sqrt{(\eta - t)(1 - 2\epsilon) - g_c(a + b)}$  and  $|\lambda_{2,i}^2| =$

Combining all the inequalities from (7), we obtain the condition of stability of the fixed point  $P$  as :

$$(a_2) \quad (\eta - t)(1 - 2\epsilon) - 1 < g_c(a + b) < 2\sqrt{\eta(1 - 2\epsilon)} - t(1 - 2\epsilon) - 1,$$

$$(b_2) \quad \eta - t - 1 < g_c(a - b) < 2\sqrt{\eta} - 1 - t.$$

**Case III :**  $\Delta_1 \geq 0$  &  $\Delta_2 < 0$

Here we have two real and one pair of complex conjugate roots of Eq. 2 and they are:

$$\begin{aligned} \lambda_{1,1}^3 &= \frac{\{1 - t(1 - 2\epsilon) - g_c(a + b)\} + \sqrt{\{t(1 - 2\epsilon) + g_c(a + b) + 1\}^2 - 4\eta(1 - 2\epsilon)}}{2}, \\ \lambda_{1,2}^3 &= \frac{\{1 - t(1 - 2\epsilon) - g_c(a + b)\} - \sqrt{\{t(1 - 2\epsilon) + g_c(a + b) + 1\}^2 - 4\eta(1 - 2\epsilon)}}{2}, \\ \lambda_{2,1}^3 &= \frac{\{1 - g_c(a - b) - t\} + i\sqrt{4\eta - \{g_c(a - b) + t + 1\}^2}}{2}, \\ \lambda_{2,2}^3 &= \frac{\{1 - g_c(a - b) - t\} - i\sqrt{4\eta - \{g_c(a - b) + t + 1\}^2}}{2}. \end{aligned} \quad (8)$$

$\sqrt{t + g_c(a - b) - \eta}, i = 1, 2$ . So the fixed point  $P$  of the system (1) will be stable if :

$$\begin{aligned} & \left\{ \begin{array}{l} \Delta_1 < 0, \\ \Delta_2 < 0, \\ |\lambda_{1,1}^2| < 1 \text{ & } |\lambda_{1,2}^2| < 1, \\ |\lambda_{2,1}^2| < 1 \text{ & } |\lambda_{2,2}^2| < 1. \end{array} \right. \\ \Rightarrow & \left\{ \begin{array}{l} |g_c(a + b) + 1 + t(1 - 2\epsilon)| < 2\sqrt{\eta(1 - 2\epsilon)}, \\ |g_c(a - b) + t + 1| < 2\sqrt{\eta}, \\ |(\eta - t)(1 - 2\epsilon) - g_c(a + b)| < 1, \\ |t + g_c(a - b) - \eta| < 1. \end{array} \right. \end{aligned} \quad (7)$$

From the above eigenvalue analysis, the stability condition for the fixed point  $P$  is as follows,

$$\begin{aligned} (a_3) \quad & |g_c(a + b) + 1 + t(1 - 2\epsilon)| \geq 2\sqrt{\eta(1 - 2\epsilon)}, \\ (b_3) \quad & (\eta - t)(1 - 2\epsilon) - 1 < g_c(a + b) < (\frac{\eta}{2} - t)(1 - 2\epsilon) + 1, \\ (c_3) \quad & \epsilon < \frac{1}{2}, \\ (d_3) \quad & \eta - t - 1 < g_c(a - b) < 2\sqrt{\eta} - 1 - t. \end{aligned}$$

**Case IV :**  $\Delta_1 < 0$  &  $\Delta_2 \geq 0$

In this case also similarly, one pair of complex conjugate and two real eigenvalues of  $J$  are :

$$\begin{aligned}
\lambda_{1,1}^4 &= \frac{\{1 - t(1 - 2\epsilon) - g_c(a + b)\} + i\sqrt{4\eta(1 - 2\epsilon) - \{t(1 - 2\epsilon) + g_c(a + b) + 1\}^2}}{2}, \\
\lambda_{1,2}^4 &= \frac{\{1 - t(1 - 2\epsilon) - g_c(a + b)\} - i\sqrt{4\eta(1 - 2\epsilon) - \{t(1 - 2\epsilon) + g_c(a + b) + 1\}^2}}{2}, \\
\lambda_{2,1}^4 &= \frac{\{1 - g_c(a - b) - t\} + \sqrt{\{g_c(a - b) + t + 1\}^2 - 4\eta}}{2}, \\
\lambda_{2,2}^4 &= \frac{\{1 - g_c(a - b) - t\} - \sqrt{\{g_c(a - b) + t + 1\}^2 - 4\eta}}{2}.
\end{aligned} \tag{9}$$

Combining all the inequalities obtained from the sign of discriminant and moduli of the four eigenvalues, we obtain the following stability condition of the fixed point  $P$  as :

- (a4)  $(\eta - t)(1 - 2\epsilon) - 1 < g_c(a + b) < 2\sqrt{\eta(1 - 2\epsilon)} - t(1 - 2\epsilon) - 1$ ,
- (b4)  $|g_c(a - b) + t + 1| \geq 2\sqrt{\eta}$ ,
- (c4)  $\eta - t - 1 < g_c(a - b) < \frac{\eta}{2} + 1 - t$ ,
- (d4)  $\eta > 0$ .

In numerical simulation, we first fix the inner and chemical synaptic coupling strengths at  $\epsilon = 0.5$  and  $g_c = 1.0$  and vary the control parameter  $\alpha$ . Figure 2

shows the different dynamics of the coupled Rulkov map which are characterized by plotting the bifurcation diagram with respect to  $\alpha$ . In Fig. 2a, the red line represents the stable steady (SS) states while green circle and blue dots correspond to the limit cycle (LC) and chaotic bursting (CB) behavior, respectively. For the fixed values of two coupling strengths  $\epsilon$  and  $g_c$ , the coupled systems converge to the stable fixed point  $P$  up to a certain threshold of  $\alpha \simeq 3.9$  and for slight increased values of  $\alpha$  the coupled systems produced the LC behavior which appear through Hopf bifurcation (HB) and sustain up to  $\alpha \simeq 4.75$ . For further increas-

**Fig. 2** **a** The bifurcation diagram and **b** variation of maximum Lyapunov exponent (MLE) of two coupled oscillator (1) with respect to  $\alpha$ . The behavior of neuron for **c**  $\alpha = 3.5$ , **d**  $\alpha = 4.2$  and **e**  $\alpha = 4.8$  illustrate stable steady state  $P$ , limit cycle and chaotic bursting, respectively

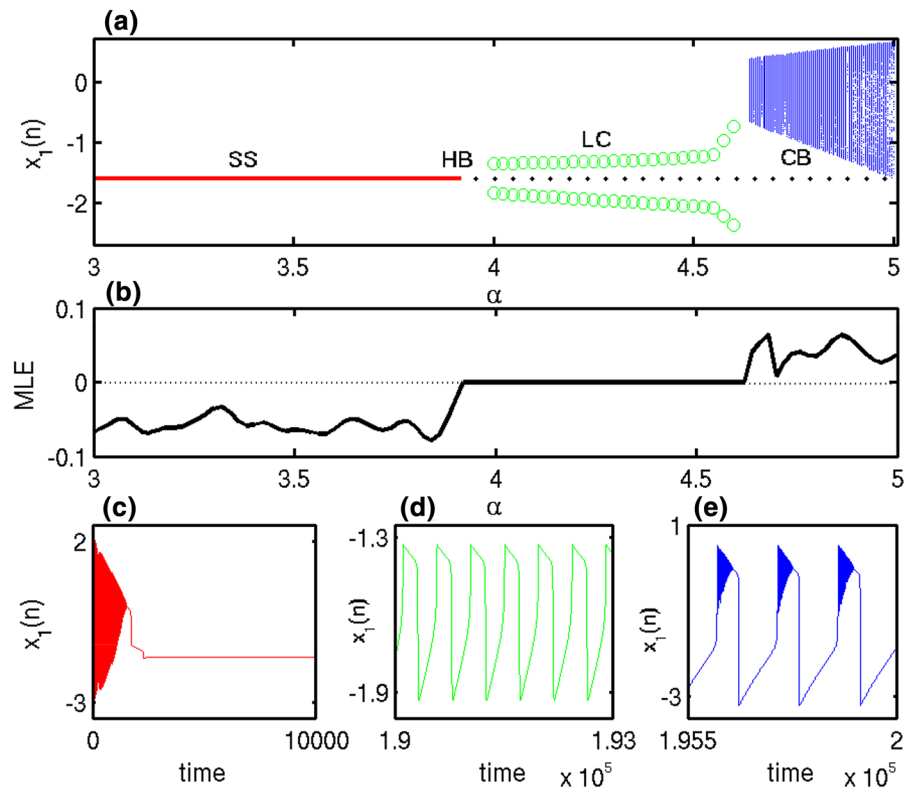
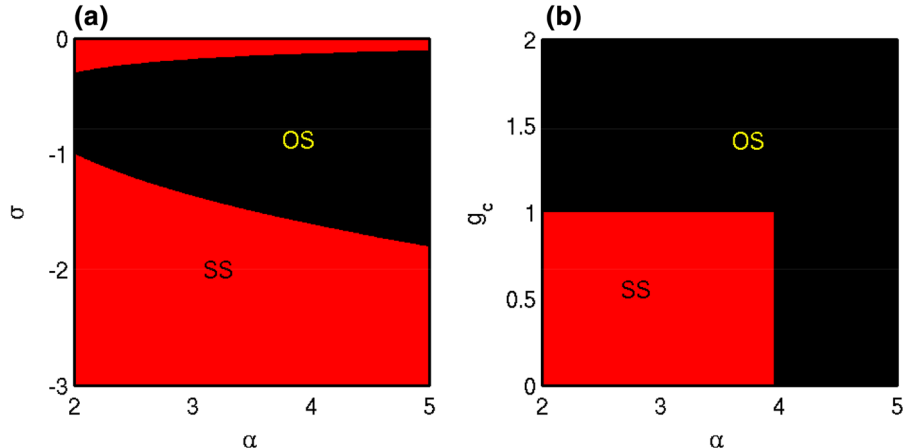


**Fig. 3** The oscillatory (OS) and steady state (SS) regions of coupled systems in **a**  $\alpha - \sigma$  plane for  $\epsilon = 0.5, g_c = 1.0$  and **b**  $\alpha - g_c$  plane for  $\sigma = -1.6, g_c = 2\epsilon$ . The red and black colors stand for SS and OS states, respectively. (Color figure online)



ing the values of  $\alpha$ , the transition takes place from LC to chaotic bursting dynamics. To characterize such collective states, the maximum Lyapunov exponent (MLE) is drawn by varying the parameter  $\alpha$  in Fig. 2b where for SS and LC states, MLE takes the negative and zero values, while for CB states MLE takes always positive value. Figure 2c–e shows the respective time evolution of three different dynamics as SS, LC and CB for  $\alpha = 3.5, \alpha = 4.2$  and  $\alpha = 4.8$ , respectively.

To reveal the complete transition scenarios form SS to oscillatory states (OS) of coupled systems, we map these collective states in the different parameter regions, as shown in Fig. 3. Using the above stability conditions, OS and SS regions are drawn in  $\alpha - \sigma$  plane in Fig. 3a for fixed coupling values  $\epsilon = 0.5$  and  $g_c = 1.0$ , where red and black colors represent the SS and OS states, respectively. Similarly, for fixed value of  $\sigma = -1.6$ , SS and OS states are plotted in  $\alpha - g_c$  plane in Fig. 3a.

#### 4 Complete synchronization (CS)

Now, we discuss the collective behavior, i.e., synchronization in the coupled system (1) in the presence of both inner linking function and chemical synapse. For this, we define the synchronization error as,

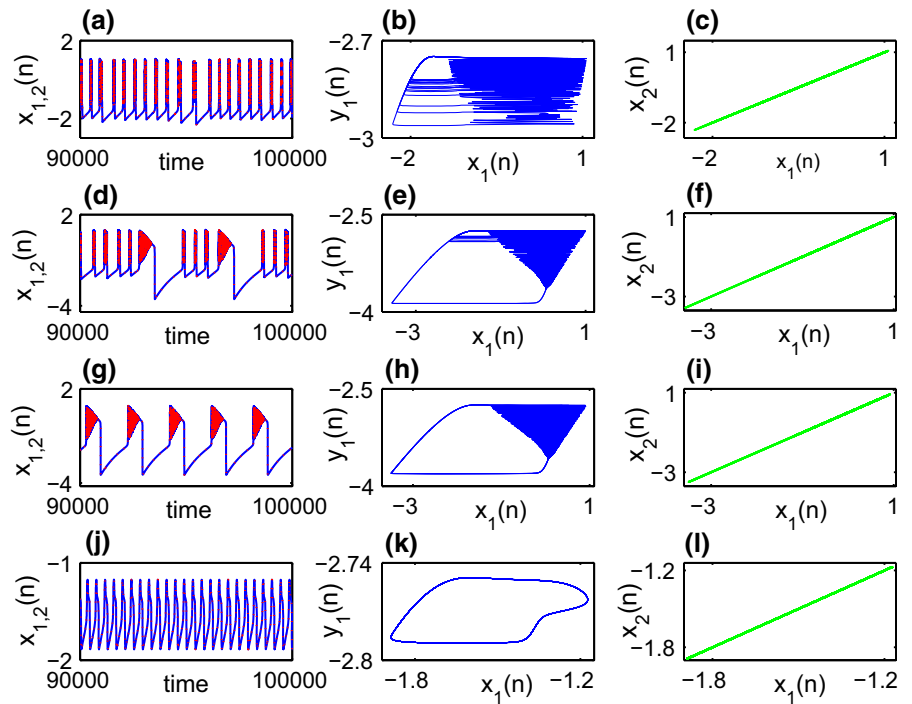
$$E = \left\langle \sqrt{(\mathbf{x}_1(n) - \mathbf{x}_2(n))^2 + (\mathbf{y}_1(n) - \mathbf{y}_2(n))^2} \right\rangle_t, \quad (10)$$

where  $\langle \cdot \rangle_t$  denotes the average over long iteration.

#### 4.1 Complete synchronization: local stability analysis

In the presence of both inner linking and chemical synaptic couplings, the coupled system achieves complete synchronization in different firing pattern forms and the results are shown in Fig. 4. The first, second and third columns represent the behavior of the neurons, phase space and corresponding synchronization manifold, respectively, for different values of chemical synaptic and inner linking coupling strengths. The coupled system oscillates in complete synchronous motion with chaotic square wave bursting for the lower values of  $g_c = \epsilon = 0.2$ . The dynamics of the  $\mathbf{x}_1(n)$  and  $\mathbf{x}_2(n)$  are represented by blue line and red dot, respectively. The chaotic square wave bursting attractor in  $(\mathbf{x}_1(n), \mathbf{y}_1(n))$  plane is presented in Fig. 4a. Figure 4c shows the corresponding synchronization manifold between the variables  $\mathbf{x}_1(n)$  and  $\mathbf{x}_2(n)$ . At this point, the other two variables  $\mathbf{y}_1(n)$  and  $\mathbf{y}_2(n)$  are also completely synchronized in chaotic square wave bursting state (figure not shown here). For increasing the values of the two coupling strengths at  $g_c = \epsilon = 0.25$ , the two neurons possess a new rich hybrid firing patterns which include the mixture of square wave and triangle bursting, and the behavior of the neurons is illustrated in Fig. 4d. The corresponding phase space and synchronization manifold are shown in Figs. 4e, f, respectively. For more increased value of  $g_c = \epsilon = 0.3$  in Fig. 4g, the neurons solely exhibited triangular firing pattern which is also manifested by the attractor in Fig. 4h. The synchronization manifold is displayed in Fig. 4i. For large increased value of the interaction strengths, each neuron attains single spike for  $g_c = 0.6, \epsilon = 0.4$

**Fig. 4** The first column represents the time series of the coupled systems for various synaptic coupling strengths, while second and third column show the phase space and the synchronized manifolds. The first, second, third and forth rows are plotted for fixed  $g_c = \epsilon = 0.2$ ;  $g_c = \epsilon = 0.25$ ;  $g_c = \epsilon = 0.3$ ; and  $g_c = 0.6, \epsilon = 0.4$ , respectively where blue line and red dot corresponds to  $\mathbf{x}_1(n)$  and  $\mathbf{x}_2(n)$ . Other parameter  $\alpha = 4.1$ . (Color figure online)



and the behavior of the neurons is displayed in Fig. 4j. The phase space dynamics of the corresponding state are drawn in Fig. 4k. The two neurons achieve the complete synchrony, and the synchronization manifold is plotted in Fig. 4l.

Now we are interested to analyze the stability of synchronize state, i.e., to determine whether the system finally returns to the synchronized state after a small perturbation from the synchronized manifold. Here we consider identical map coupled by bidirectional chemical synapse and inner coupling. So, the stability criterion for synchronization can be accounted by master stability function (MSF) methodology [44], which gives the necessary condition for stability of the synchronous solution. In our case, the equation of motion of two identical Rulkov coupled maps in the presence of both chemical synapse and inner linking function becomes,

$$\begin{aligned} \mathbf{x}_1(n+1) &= f(\mathbf{x}_1(n), \mathbf{y}_1(n), \alpha) \\ &+ g_c(v_s - \mathbf{x}_1(n))\Gamma(\mathbf{x}_2(n)) \\ &+ \epsilon[f(\mathbf{x}_2(n), \mathbf{y}_2(n), \alpha) \\ &- f(\mathbf{x}_1(n), \mathbf{y}_1(n), \alpha)], \end{aligned}$$

$$\mathbf{y}_1(n+1) = \mathbf{y}_1(n) - \eta(\mathbf{x}_1(n) - \sigma),$$

$$\mathbf{x}_2(n+1) = f(\mathbf{x}_2(n), \mathbf{y}_2(n), \alpha)$$

$$\begin{aligned} &+ g_c(v_s - \mathbf{x}_2(n))\Gamma(\mathbf{x}_1(n)) \\ &+ \epsilon[f(\mathbf{x}_1(n), \mathbf{y}_1(n), \alpha) \\ &- f(\mathbf{x}_2(n), \mathbf{y}_2(n), \alpha)], \end{aligned}$$

$$\mathbf{y}_2(n+1) = \mathbf{y}_2(n) - \eta(\mathbf{x}_2(n) - \sigma), \quad (11)$$

where  $f(\mathbf{x}, \mathbf{y}, \alpha) = \frac{\alpha}{1+\mathbf{x}^2} + \mathbf{y}$ ,  $\Gamma(\mathbf{x}) = \frac{1}{1+\exp(-k(\mathbf{x}-\Theta_s))}$ . When synchronization occurs, let the  $i$ -th ( $i = 1, 2$ ) oscillator evolves synchronously with  $(\mathbf{x}_i(n), \mathbf{y}_i(n)) = (\mathbf{x}(n), \mathbf{y}(n))$ . Now perturb the  $i$ -th node from its synchronization manifold with small amount  $(\delta\mathbf{x}_i(n), \delta\mathbf{y}_i(n))$ , so the current state of this node can be written as  $(\mathbf{x}_i(n), \mathbf{y}_i(n)) = (\mathbf{x}(n) + \delta\mathbf{x}_i(n), \mathbf{y}(n) + \delta\mathbf{y}_i(n))$ .

Considering small perturbation and expanding around the synchronous solution  $(\mathbf{x}(n), \mathbf{y}(n))$  up to the first order of  $(\delta\mathbf{x}_i(n), \delta\mathbf{y}_i(n))$ , we get the linearized equations of the error systems of Eq. (11) as,

$$\begin{aligned} \delta\mathbf{x}_1(n+1) &= (1-\epsilon)[f_x(\mathbf{x}(n), \mathbf{y}(n), \alpha)\delta\mathbf{x}_1(n) \\ &+ f_y(\mathbf{x}(n), \mathbf{y}(n), \alpha)\delta\mathbf{y}_1(n)] \\ &+ \epsilon[f_x(\mathbf{x}(n), \mathbf{y}(n), \alpha)\delta\mathbf{x}_2(n) \\ &+ f_y(\mathbf{x}(n), \mathbf{y}(n), \alpha)\delta\mathbf{y}_2(n)] \\ &+ g_c(v_s - \mathbf{x}(n))\Gamma_x(\mathbf{x}(n))\delta\mathbf{x}_2(n) \\ &- g_c\Gamma(\mathbf{x}(n))\delta\mathbf{x}_1(n), \end{aligned}$$

$$\delta\mathbf{y}_1(n+1) = \delta\mathbf{y}_1(n) - \eta\delta\mathbf{x}_1(n),$$

$$\delta\mathbf{x}_2(n+1) = (1-\epsilon)[f_x(\mathbf{x}(n), \mathbf{y}(n), \alpha)\delta\mathbf{x}_2(n)$$

$$\begin{aligned}
& + f_y(\mathbf{x}(n), \mathbf{y}(n), \alpha) \delta \mathbf{y}_2(n) \\
& + \epsilon [f_x(\mathbf{x}(n), \mathbf{y}(n), \alpha) \delta \mathbf{x}_1(n) \\
& + f_y(\mathbf{x}(n), \mathbf{y}(n), \alpha) \delta \mathbf{y}_1(n)] \\
& + g_c(v_s - \mathbf{x}(n)) \Gamma_x(\mathbf{x}(n)) \delta \mathbf{x}_1(n) \\
& - g_c \Gamma(\mathbf{x}(n)) \delta \mathbf{x}_2(n), \\
\delta \mathbf{y}_2(n+1) & = \delta \mathbf{y}_2(n) - \eta \delta \mathbf{x}_2(n).
\end{aligned} \tag{12}$$

Among four Lyapunov exponents of the above master stability equation (12), two Lyapunov exponents are parallel to the synchronization manifold and the directions of the other two are transverse to it.

In this case, the two Rulkov models are coupled by bidirectional inner linking function and chemical synapses. So the adjacency and Laplacian matrices of the chemical synaptic layer are, respectively,  $\mathcal{A}^{(c)} = \begin{bmatrix} 0 & 1 \\ 1 & 0 \end{bmatrix}$ , and  $\mathcal{L}^{(c)} = \begin{bmatrix} 1 & -1 \\ -1 & 1 \end{bmatrix}$ . The eigenvalues of the Laplacian matrix  $\mathcal{L}^{(c)}$  are 0 and 2 with respective eigenvectors  $\begin{bmatrix} V_{11}^c \\ V_{12}^c \end{bmatrix} = \begin{bmatrix} \frac{1}{\sqrt{2}} \\ \frac{1}{\sqrt{2}} \end{bmatrix}$  and  $\begin{bmatrix} V_{21}^c \\ V_{22}^c \end{bmatrix} = \begin{bmatrix} \frac{1}{\sqrt{2}} \\ -\frac{1}{\sqrt{2}} \end{bmatrix}$ . The direction of the eigenvector corresponding to the eigenvalue 0 is parallel to the synchronization manifold, another one be the transverse direction. To detect the two transverse Lyapunov exponents, we project  $(\delta \mathbf{x}_i(n), \delta \mathbf{y}_i(n))$ ,  $i = 1, 2$  onto the basis of eigenvectors. Let  $(\xi_i^{(x)}(n), \xi_i^{(y)}(n))$  be the projection of the synchronization error vector onto the space spanned by Laplacian eigenvectors. Then

$$\begin{aligned}
\xi_1^{(x)}(n+1) & = \sum_{j=1}^2 V_{1j}^c \delta \mathbf{x}_j(n+1) \\
& = \frac{1}{\sqrt{2}} [\delta \mathbf{x}_1(n+1) + \delta \mathbf{x}_2(n+1)] \\
& = f_x(\mathbf{x}(n), \mathbf{y}(n), \alpha) \xi_1^{(x)}(n) \\
& + f_y(\mathbf{x}(n), \mathbf{y}(n), \alpha) \xi_1^{(y)}(n) \\
& + g_c(v_s - \mathbf{x}(n)) \Gamma_x(\mathbf{x}(n)) \xi_1^{(x)}(n) \\
& - g_c \Gamma(\mathbf{x}(n)) \xi_1^{(x)}(n), \\
\xi_1^{(y)}(n+1) & = \sum_{j=1}^2 V_{1j}^c \delta \mathbf{y}_j(n+1) \\
& = \xi_1^{(y)}(n) - \eta \xi_1^{(x)}(n),
\end{aligned} \tag{13}$$

and

$$\begin{aligned}
\xi_2^{(x)}(n+1) & = \sum_{j=1}^2 V_{2j}^c \delta \mathbf{x}_j(n+1) \\
& = \frac{1}{\sqrt{2}} [\delta \mathbf{x}_1(n+1) - \delta \mathbf{x}_2(n+1)] \\
& = (1 - 2\epsilon) [f_x(\mathbf{x}(n), \mathbf{y}(n), \alpha) \xi_2^{(x)}(n) \\
& + f_y(\mathbf{x}(n), \mathbf{y}(n), \alpha) \xi_2^{(y)}(n)] \\
& - g_c(v_s - \mathbf{x}(n)) \Gamma_x(\mathbf{x}(n)) \xi_2^{(x)}(n) \\
& - g_c \Gamma(\mathbf{x}(n)) \xi_2^{(x)}(n), \\
\xi_2^{(y)}(n+1) & = \sum_{j=1}^2 V_{2j}^c \delta \mathbf{y}_j(n+1) \\
& = \xi_2^{(y)}(n) - \eta \xi_2^{(x)}(n).
\end{aligned} \tag{14}$$

Clearly Eq. (13) be the linearized equation parallel to the synchronized manifold. So our required master stability equation transverse to the synchronized manifold is Eq. (14).

The partial derivatives for two coupled network are evaluated as  $f_x(\mathbf{x}(n), \mathbf{y}(n), \alpha) = \frac{-2\alpha \mathbf{x}(n)}{(1+\mathbf{x}^2(n))^2}$ ,  $f_y(\mathbf{x}(n), \mathbf{y}(n), \alpha) = 1$ ,  $\Gamma_x(\mathbf{x}(n)) = \frac{k \exp\{-k(\mathbf{x}(n) - \Theta_s)\}}{[1 + \exp\{-k(\mathbf{x}(n) - \Theta_s)\}]^2}$ .

Finally, our required MSE transverse to the synchronization manifold is

$$\begin{aligned}
\xi^{(x)}(n+1) & = (1 - 2\epsilon) \left[ \frac{-2\alpha \mathbf{x}(n)}{(1+\mathbf{x}^2(n))^2} \xi^{(x)}(n) + \xi^{(y)}(n) \right] \\
& - g_c \frac{\xi^{(x)}(n)}{1 + \exp\{-k(\mathbf{x}(n) - \Theta_s)\}} \\
& + g_c \frac{k(\mathbf{x}(n) - v_s) \exp\{-k(\mathbf{x}(n) - \Theta_s)\}}{[1 + \exp\{-k(\mathbf{x}(n) - \Theta_s)\}]^2} \\
& \xi^{(x)}(n), \\
\xi^{(y)}(n+1) & = -\eta \xi^{(x)}(n) + \xi^{(y)}(n),
\end{aligned} \tag{15}$$

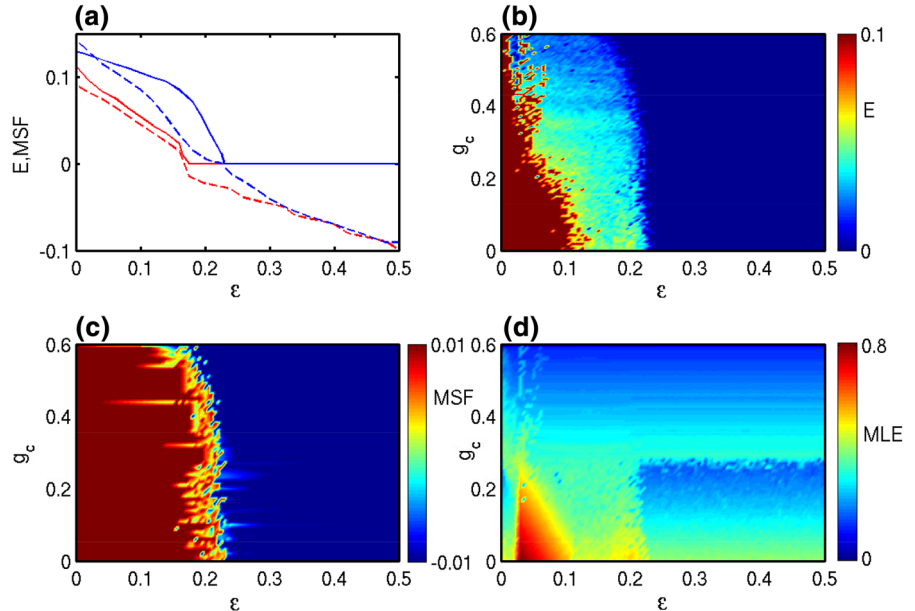
where  $\mathbf{x}(n)$  and  $\mathbf{y}(n)$  be the state variables for synchronized system obeying

$$\begin{aligned}
\mathbf{x}(n+1) & = \frac{\alpha}{1 + \mathbf{x}^2(n)} + \mathbf{y}(n) \\
& - g_c \frac{(\mathbf{x}(n) - v_s)}{1 + \exp\{-k(\mathbf{x}(n) - \Theta_s)\}},
\end{aligned} \tag{16}$$

$$\mathbf{y}(n+1) = \mathbf{y}(n) - \eta(\mathbf{x}(n) - \sigma).$$

The MLE of the MSE (15) as a function of the parameter  $g_c$  and  $\epsilon$  gives the necessary condition for the stability of the synchronous solution, and the synchronous state is stable if the value of MLE is negative.

**Fig. 5** Variation of **a** synchronization error (solid line) and the master stability function (MSF) (dashed line) by changing the inner coupling strength  $\epsilon$  for fixed values of chemical synaptic coupling strength  $g_c = 0.01$  (blue color) and  $g_c = 0.59$  (red color). Two parameter region for synchronization in the  $\epsilon - g_c$  parameter space where color bar represents the variation of **b** synchronization error  $E$  and **c** MSF. The local dynamics of each systems is characterized through MLE in **d**. Here  $\alpha = 4.1$ . (Color figure online)



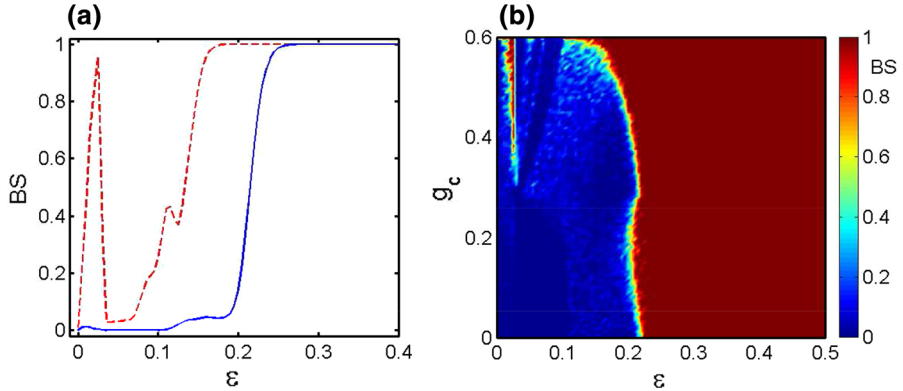
The complete scenario of the neuronal synchrony in the different firing patterns and their robustness are shown in Fig. 5. The enhancement of neuronal synchrony of coupled oscillators is characterized by plotting the synchronization error (solid line) and the MSF (dashed line) in Fig. 5a by varying the inner coupling strength  $\epsilon$  for two different fixed values of chemical synaptic coupling strength  $g_c$ . The solid and dashed blue lines represent the synchronization error ( $E$ ) and the MSF keeping the chemical coupling strength fixed at  $g_c = 0.01$  for which complete synchrony occurs at the critical inner coupling strength  $\epsilon_c = 0.23$ . At this critical coupling strength, the synchronization error  $E$  becomes zero and MSF crosses to zero line from positive to negative. If we increase the value of chemical coupling strength at  $g_c = 0.59$ , the critical inner coupling strength  $\epsilon_c = 0.175$  is lower from the previous value for the complete synchrony. So from this figure, it is noted that if the interaction strength of chemical synapses is increased then the critical value of inner function strength decreases, i.e., enhancement of complete synchrony [52,53] occurred. To show the enhancing synchrony, we simultaneously change the values of inner and synaptic coupling strength in the  $\epsilon - g_c$  parameter space for the range of  $\epsilon \in [0.0, 0.5]$  and  $g_c \in [0.0, 0.6]$ . We change both  $\epsilon$  and  $g_c$  with a step size of 0.005. It is clear from parameter region in Fig. 5b that the critical value of inner linking coupling strength  $\epsilon_c$  decreases with increasing the value

of synaptic coupling strength  $g_c$ . The deep blue region corresponds to the complete synchronous state in which synchronization error  $E$  takes the value 0. This scenario is confirmed by calculating the values of MSF in Fig. 5c where simultaneously varying both the coupling strengths. From this figure, it is noted that the analytical condition derived by master stability approach excellently matches with our numerical results. Through the MLE characterization, we investigate the local dynamics of the each dynamical unit of the coupled systems in  $\epsilon - g_c$  plane. The results are depicted in Fig. 5d, and it shows that increasing values of the chemical synaptic coupling strength  $g_c$  leads to the more regular behavior of each system.

#### 4.2 Complete synchronization: global stability analysis

The coexistence of different stable states for a given set of parameters of a dynamical systems is known as multistability, and this features plays a crucial role in cell signaling and the neuronal interaction [54,55]. The multi-stable behavior in a coupled neuronal network mainly appears due to the different initial condition of the states, and the several neuronal important ingredients like synaptic coupling [56], time-delayed interaction [57,58], phase locking parameter [59], etc., introduced such features. The multistability and bifur-

**Fig. 6** **a** Variation of basin stability by varying the inner coupling strength  $\epsilon$  for synaptic coupling strength  $g_c = 0.01$  (solid blue line) and  $g_c = 0.59$  (dashed red line). **b** The parameter region for synchronization in  $\epsilon - g_c$  plane where variation of basin stability measure is used in color bar. (Color figure online)



cation analysis were studied in two coupled neurons in the presence of multiple delays [60–62], and also the corresponding dynamics were discussed. Using perturbation technique, the existence of multiple solutions was investigated analytically [63]. The multistability phenomena is a mimic of different brain states operating on a particular object. The existence of multiple functioning regimes is necessary for brain function, and the role of multifarious dynamical regimes in neuronal interactions has been investigated theoretically and experimentally [54]. So, for the neuronal point of view, it is very important to quantify the dynamical regimes of multi-stable states. In this context, we use the basin stability (BS) [46, 48] frame work to quantify the different states in coupled neuronal systems. The basin stability is defined as

$$\text{BS} = \int_{\mathcal{B}} \chi(x) \rho(x) dx, \quad (17)$$

where  $\mathcal{B}$  is the set of possible perturbed states  $x$ ,  $\chi(x) = 1$  if the system converges to synchronized states after perturbation  $x$  and zero otherwise,  $\rho(x)$  be the density of the perturbed states with  $\int_{\mathcal{B}} \rho(x) dx = 1$ . For computing BS numerically, we simulate the whole system for  $T$  (sufficiently large number) different initial conditions drawn uniformly random from its phase space, and let the number of initial conditions that finally arrive at synchronous state is  $M$ . Then, the BS for the synchronous state is calculated as  $\frac{M}{T}$ , which belongs to  $[0, 1]$ . BS = 0 means that for any random initial condition, the synchronization state is unstable and it is globally stable for BS = 1.0, while  $0 < \text{BS} < 1.0$  corresponds to the probability of getting the synchronous states for any random initial condition from its phase space. To check the global stability of

the synchronous state, we draw its BS in Fig. 6 by taking large number of initial conditions from their basin volume  $[-2.5, 1.5] \times [-3, -2]$ . The variation of the BS against the inner coupling strength  $\epsilon$  is shown in Fig. 6a. The solid blue line and dashed red line correspond to the two different chemical synaptic coupling strength as  $g_c = 0.01$  and  $g_c = 0.59$ , respectively. In both cases, BS gradually increases from 0 to 1 with the increasing values of  $\epsilon$  in which for the lower values of the  $\epsilon$ , BS takes the values close to 0 which means there is a very small number of fraction of initial conditions in the basins volume for which the complete neuronal synchrony will appear while after a certain threshold value of  $\epsilon$ , BS takes the value 1 which refers that complete synchrony is achieved for all initial conditions in the basin volume. The coexistence of the neuronal synchrony and de-synchrony appears in a narrow region of the parameter space where BS lies in (0,1). Also it has been noted that enhancement of the complete neuronal synchrony is quantified by the BS measurement since for chemical synaptic coupling  $g_c = 0.59$ , BS reaches at 1 values at the coupling strength  $\epsilon = 0.18$  (red dashed line) which is lower compared to the critical values of  $\epsilon = 0.26$  (solid blue line) for  $g_c = 0.01$ . From this figure, it is concluded that complete neuronal synchrony and its enhancement occur in a global sense. Figure 6b shows the global stability and enhancement of the complete neuronal synchrony in the  $\epsilon - g_c$  parameter space where color bar shows the variation of BS. The deep red and blue colors represent the complete synchronous and desynchronous region, whereas the mixing colors correspond to the coexisting states. It can be seen that the stability of the synchronous states increases considerably as the synaptic coupling strength  $g_c$  increases. In Fig. 6b, the narrow synchrony

nization region is observed in the lower values of inner coupling strength  $\epsilon \simeq 0.02$  for  $g_c \in (0.39, 0.6]$  and the corresponding BS variation shows in Fig. 6a (dashed red line), and this happened due to the presence of multistability features of the coupled systems.

## 5 Effect of different types of interactions on complete synchronization

In this section, we study the effect of different types of interactions such as time-delayed effect, blinking interaction and autaptic effect on the neural synchronization.

### 5.1 Time delay in the neuronal interaction

We study the effect of time delay in the coupling function as time delay interaction arises for transmitting information signals from pre-synaptic to post-synaptic of the neurite. When a constant delay  $\tau \in \mathbb{N} \cup \{0\}$  is inaugurated to the inner linking function, then the net current flowing to the  $i$ -th neuron from  $j$ -th through inner coupling is  $[f(\mathbf{x}_j(n - \tau), \mathbf{y}_j(n - \tau), \alpha) - f(\mathbf{x}_i(n), \mathbf{y}_i(n), \alpha)]$ , and for delay induced chemical interaction we can adopt  $\Gamma(\mathbf{x}(n))$  as  $\Gamma(\mathbf{x}(n)) = \frac{1}{1 + \exp[-k(\mathbf{x}(n - \tau) - \Theta_s)]}$ . Here we found that the presence of time delay in the only inner coupling induced the enhancement neuronal synchrony in the whole region of coupling strength and the delay time. While we interestingly found that the presence of delay time in both the interactions induced enhancement of synchrony up to a certain values of  $\tau$  and after this threshold time delay induced the de-enhancement. For these, we consider three different cases, first we study the effect of time delay on synchronization when only inner coupling function is delayed form. In this position, we assume the chemical transmission from pre-synaptic synapse to post-synaptic synapse as instantaneous. Our main emphasis is to identify the parameter region in coupling strength and time delay  $\tau$  for the emergence of synchronization. We vary both the inner and chemical coupling strengths as a function of another parameter  $\mu$  by the relation  $\mu = g_c = 2\epsilon$  in order to simultaneously vary both the interaction strengths in appropriate proportion. Figure 7a shows the synchronization and desynchronization region in the  $\mu - \tau$  parameter space. Here synchronization error

$E$  is used to distinguish synchronization and desynchronization states. The critical coupling strength  $\mu$  for the complete synchronization gradually decreases by increasing values of inner linking delay time  $\tau$  so enhancing of synchrony is observed. But the presence of time delay in the only chemical synaptic function does not have effect on the neural synchronization, only synaptic coupling strength determine the neural synchrony, scenario shown in Fig. 7b. Next we introduce time delay in both the coupling functions, namely inner and synaptic coupling. Then, it is interestingly noticed that the presence of time delay in the both coupling, the enhancement of the neuronal synchrony is possible up to a certain threshold of the time delay  $\tau = 13.0$  and further increased values of the delay time induced the de-enhancement of synchrony in Fig. 7c. The stability of the neuronal enhancement and de-enhancement of synchronous state are quantified by the basin stability measurement which are plotted in Fig. 7d–f corresponding to Fig. 7a–c, respectively. For the calculation of basin stability, we chose the initial basin as  $[-2.5, 1.5] \times [-3, -2]$  in which the amplitude of the uncoupled neuron lies. From Fig. 7d–f, it is shown that the deep red color takes the value 1 in the color bar which means the neural synchrony solely appears in that set of parameter region in  $\mu - \tau$  space for all initial conditions from the prescribed phase space while the mixture color shows the coexisting of synchrony and de-synchrony. Due to the multisatibility of the coupled systems, the narrow synchronization island is seen in Fig. 7d, f using BS measure. The deep blue color represents the desynchronization dynamics for all initial conditions as it takes the values 0 of the color bar. Moreover the neuronal synchronization appears for all the initial condition from the prescribed basin for a certain range of coupling strength ( $\mu$ ) and time delay ( $\tau$ ) and after increasing  $\mu$  and  $\tau$  coexistence region is observed. Interestingly, the presence of time delay only in the inner linking function shows the less coexistence region of neural synchrony and de-synchrony in  $\mu - \tau$  parameter space compared to the presence of delay in both the interactions.

### 5.2 On–off neuronal coupling scheme

This section is devoted for the study of neuronal synchronization in the presence of on–off interaction over time, and these types of coupling have great relevance

**Fig. 7** Two-parameter phase space diagram in  $\mu - \tau$  plane in the presence of time delay  $\tau$  in: **a, d** inner coupling function and **b, e** chemical synaptic interaction only and **c, f** both coupling functions. Color bar of synchronization error  $E$  and basin stability BS measure are used to distinguish different states in the first and second rows, respectively. (Color figure online)

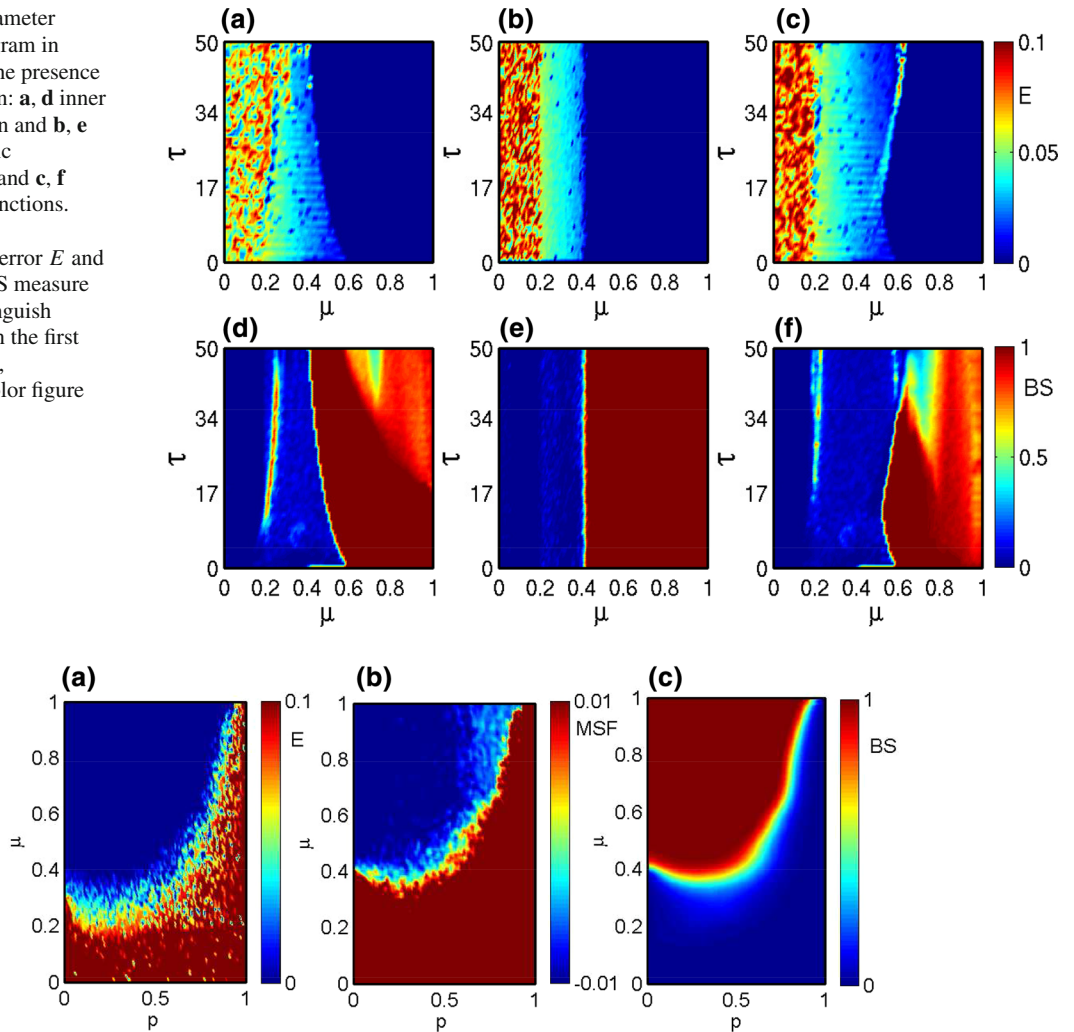


**Fig. 8** The fully synchronized and desynchronized regions are plotted by simultaneous varying on-off interaction probability  $p$  and coupling strength  $\mu = g_c = 2\epsilon$ . The color bars show

the variation of **a** synchronization error  $E$ , **b** MSF and **c** basin stability measurement to identify the synchronous state in  $p - \mu$  parameter space. (Color figure online)

in the field of neuroscience. Such types of interactions are usually seen in the inter-neuronal communications, since during this time one neuron produces spike to send out a electrical signal to the other neuron and the interaction takes place through the synapses during the arrival of the spike where the spike duration is very small compared to the inter-spike interval, and this phenomena can be presented by *on-off* interaction. Also neuronal interaction does not happen spontaneously since the signals transfer from one to another neuron may interrupt for some time period. This feature promotes the removal of connection between two neurons. Belykh et al. [64] studied the synchronization

phenomenon in blinking time-varying interaction. To investigate the synchrony of the coupled neurons, we stochastically implement this time varying on-off character for which a parameter  $p$  is introduced. At each iteration with probability  $p$ , the chemical and inner coupling connections remove independently.  $p = 0$  implies that the two neurons are always connected through both the synapses, whereas if  $p = 1$ , they are disconnected for all time iteration. Remarkably, we observe that for lower values of  $p$  the complete synchronization attains at the lower values of the synaptic coupling strength  $\mu$ . For higher values of  $p$ , the critical synaptic coupling strength for the complete neuronal

synchrony monotonically increases and persists up to a certain threshold of  $p$ . Beyond this critical value of  $p$ , no synchronization is possible for any synaptic coupling strength  $\mu$  and this phenomenon is delineated in color coded Fig. 8a, where the color bar shows the variation of synchronization error and blue color region represents the fully synchronized domain in the  $p - \mu$  parameter space. The stability of the synchronous state is explained in Fig. 8b by the MLE of the master stability equation 15. Further quantification of stable synchronous state, we calculate the basin stability measure, plotted in Fig. 8c. The color bar illustrates the variation of BS, where the BS rises smoothly from the lower values of coupling strength and finally indicates the mono-stable synchronous states. On the other hand, after certain value of coupling strength it decreases gradually as the link removing probability  $p$  increases.

### 5.3 Autapse-induced neuronal synchrony

In this section, we study the autapse effect in the neuronal synchrony in coupled oscillators. Autapse is a special type synaptic structure which is an self-synapse and connects a neuron to itself. The autaptic synaptic transmission takes place between the axon and soma of the same neuron in the nervous systems as form a time-delayed self-feedback mechanism. In the presence of a constant autaptic delay  $\tau_a$ , the autaptic inner linking function is taken as  $[f(x_i(n - \tau_a), y_i(n - \tau_a), \alpha) - f(x_i(n), y_i(n), \alpha)]$  and the chemical autaptic function as  $(v_s - x_i(n))\Gamma(x_i(n - \tau_a))$ , are additionally added to  $x_1$  and  $x_2$  variables of the first and second nodes in Eq. (11) with respective synaptic strength  $\epsilon$  and  $g_c$ . The schematic representation of the autaptic interaction is shown in Fig. 9, where  $\tau_a$  and  $\tau$  denote the autaptic transmission delay and the synaptic coupling delay with corresponding chemical synaptic coupling strength  $g_c$  and inner coupling strength  $\epsilon$ . This unfamiliar type of synapse is first explored by Van der Loos and Glaser [39] and named it as an *autapse*. After that the existence of such synapse were verified by several experimental techniques [65–67]. Autaptic connection induces an additional timescale to several neuronal activities and causing various dynamical features in neurons. Also the irregular neuronal firing can be regulated through inhibitory autaptic transmission [68]. The combined effect of electrical and chemical synapses induced multiple coherence resonance in sin-

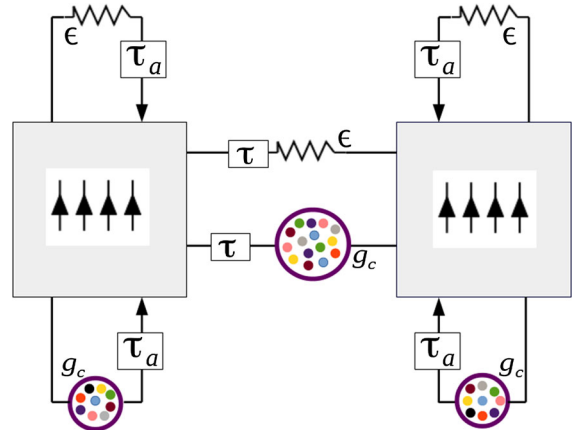
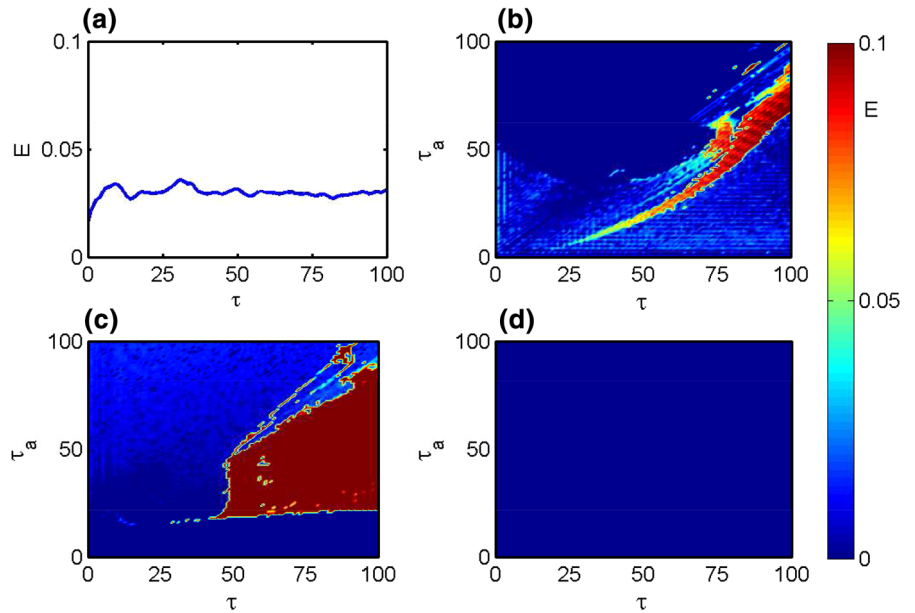


**Fig. 9** The schematic diagram of autaptic transmission in the coupled neuronal system

gle stochastic Hodgkin-Huxley neurons, and scale-free neuronal networks are investigated [69].

In our study, we consider the chemical synaptic and inner feedback delayed autapse in the presence of inner linking and chemical synaptic function of two coupled neuronal Rulkov maps. We found that autaptic delay plays a key role to achieve the complete neural synchrony in neural network. It is shown that certain amount of autaptic delay induced the complete neural synchrony whereas in the absence of any type of autaptic connection, no complete neural synchronization is possible as shown in Fig. 10a. The synchronization error (E) is plotted in Fig. 10a against the synaptic coupling delay  $\tau$  with fixed synaptic coupling strength  $\epsilon = 0.2$ ,  $g_c = 0.4$  and in the absence of autaptic connection. It is easily shown that the synchronization error never converges to zero for all synaptic coupling delay which refers to the complete desynchronized regime. But when autaptic delayed ( $\tau_a$ ) is introduced only in the inner feedback synapse, the complete neuronal synchronization is appeared and remarkably it enhances the synchrony for its higher values. The clear picture of synchronization region in the  $\tau - \tau_a$  parameter space is shown in Fig. 10b. Here the color bar shows the variation of the synchronization error for which the deep blue region corresponds to the fully synchronized regime as it takes the 0 value whereas other color represents the desynchronized region. Next, if we introduce the same amount of delay in the chemical synaptic autapse instead of inner feedback synapse, then also neural synchrony exists in a small region of  $\tau - \tau_a$  parameter space compared to the previous one

**Fig. 10** Autapse-induced neuronal synchrony: **a** variation of synchronization error by varying the transmission delay  $\tau$  in absence of autapses. The parameter space in  $\tau - \tau_a$  plane for neuronal synchrony in the presence of **b** only inner autapse, **c** solely chemical autapse and **d** both types of autapses. (Color figure online)



and the results are shown in Fig. 10c. From Fig. 10b, it is clearly shown that by increasing on the autaptic delay in electrical synapse induced the neural synchrony and persists but have opposite scenario in the case of chemical synapse (Fig. 10c). In the presence of same amount of autaptic delay in both the synapses also induce the fully complete synchronized region and also shows rapid enhancement (Fig. 10d) in the  $\tau - \tau_a$  parameter space.

To check the global stability of the synchronize state as in Fig. 10, we calculate the basin stability measure to identify the effect of initial condition. Figure 11 shows the global stability parameter region by changing the delayed parameters  $\tau$  and  $\tau_a$  simultaneously. The color bar in Fig. 11 shows the variation of the basin stability where the deep blue, red and mixing of different colors represent the corresponding fully desynchronized, synchronized and coexistence region, respectively. Our results on the effect of autapse provide an insightful mechanistic understanding of how different types of autapses shape influence the neuronal synchrony or not. Autapses connect the neurons in a local area and induce the neuronal synchrony in between two coupled neurons.

## 6 Different types of neuronal dynamical states

Neurons are excitable units that can emit spike or different types of burst of electrical as well as chemical

signals which means the systems are in stable steady states behavior, but when it is excited beyond a critical threshold, it transmit a pulse. In the following section, we investigate the transition among different dynamical states of coupled neurons which refer to the case where one uncoupled neuron is in silence mode and other one is in firing pattern. Then, depending on the two types couplings and controlling parameters, the individual oscillator showing the same as well as different types of firing patterns and this type of phenomenon are closely related to the several neuronal processes. The typical time evolution for different dynamics such as bursting, synchronized and desynchronized spiking steady state is illustrated in Fig. 12. In the absence of any interaction (i.e.,  $g_c = \epsilon = 0.0$ ), the isolated map exhibits the steady state and square wave bursting behavior in Fig. 12a for the fixed value of control parameter  $\alpha_1 = 3.9$  and  $\alpha_2 = 4.1$  where solid blue and dotted red lines represent the evolution of  $\mathbf{x}_1(n)$  and  $\mathbf{x}_2(n)$  states, respectively. Next we are interested to observe the behavior of neurons in the presence of nonzero coupling strengths for fixed value of control parameter. For lower value of coupling strength  $g_c = 0.02$  and  $\epsilon = 0.01$ , it is shown in Fig. 12b that the silence mode neuron which was steady state dynamics transit to the triangular firing pattern while square wave bursting dynamics is qualitative same. For further tuning values of the interaction strengths at  $g_c = 0.02$  and  $\epsilon = 0.5$ , the two neurons are firing with the same pattern in coherence

**Fig. 11** The global stability of the synchronization state in Fig. 10: **a** variation of basin stability with respect to  $\tau$  in the absence of any autapse. Global stability of the neuronal synchrony in  $\tau - \tau_a$  parameter space in the presence of **b** only inner autapse, **c** solely chemical autapse and **d** both types of autapses. (Color figure online)

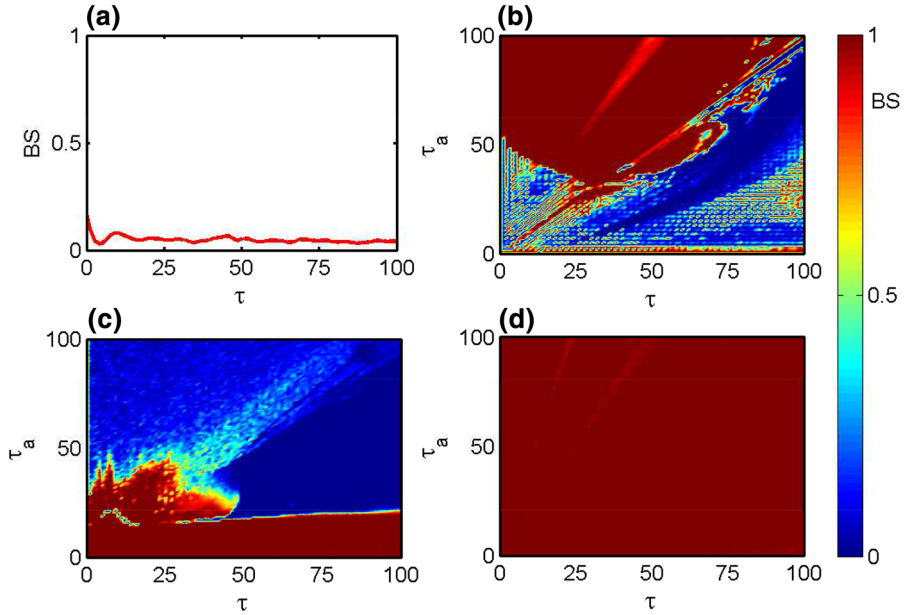
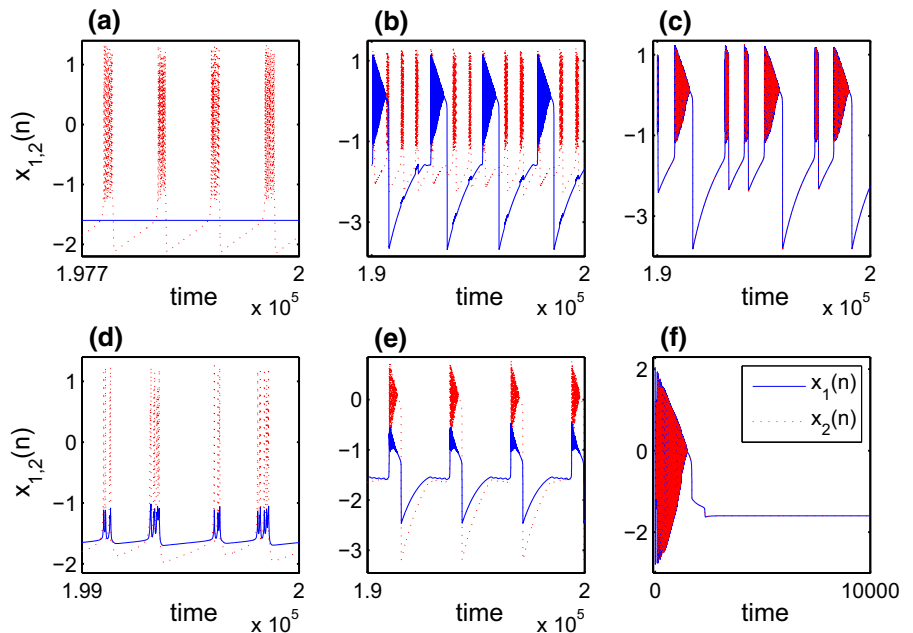


**Fig. 12** The upper and lower row show the time series of the coupled oscillators for two different set of controlling parameters as  $\alpha_1 = 3.9, \alpha_2 = 4.1$ , and  $\alpha_1 = 2.1, \alpha_2 = 4.8$ , respectively. The various coupling parameters are used: **a**  $g_c = \epsilon = 0$ , **b**  $g_c = 0.02, \epsilon = 0.01$ , **c**  $g_c = 0.02, \epsilon = 0.5$ , **d**  $g_c = 0.2, \epsilon = 0.1$ , **e**  $g_c = 0.4, \epsilon = 0.2$  and **f**  $g_c = 1.0, \epsilon = 0.5$ . (Color figure online)

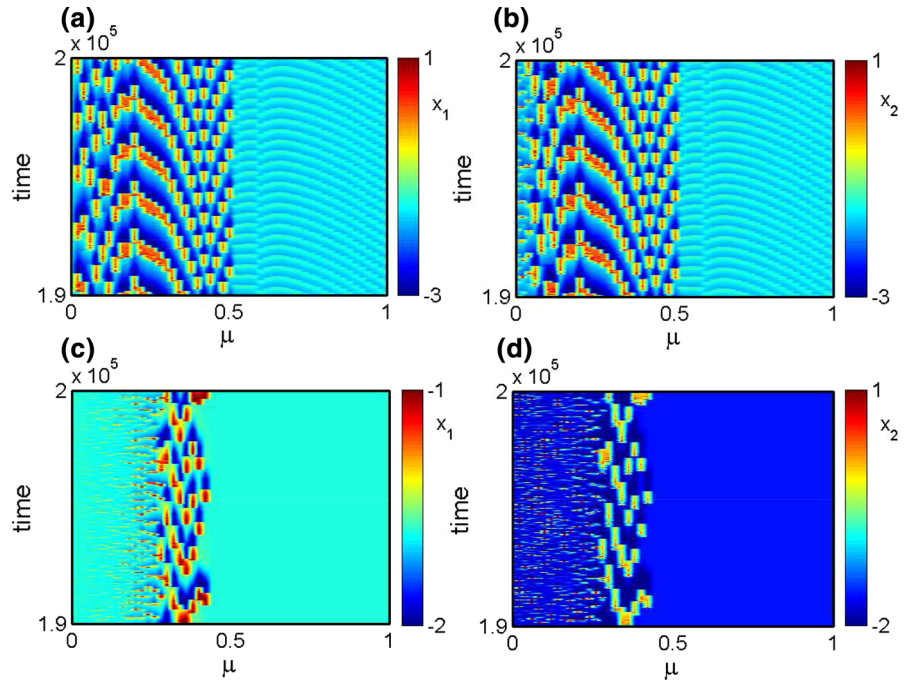


motion drawn in Fig. 12c. Next we choose other set of system parameter as  $\alpha_1 = 2.1$  and  $\alpha_2 = 4.8$ , and one neuron is in silence mode and other one is in bursting firing pattern in the absence of interaction (figure is not shown). With the tuning of two coupling strengths, both the time series of both the neurons are in phase locked state with square wave and triangular bursting patterns for  $g_c = 0.2, \epsilon = 0.1$  and  $g_c = 0.4, \epsilon = 0.2$  in

Figs. 12d, e, respectively. Finally, both the neurons are converged to the silence mode by tuning the coupling strengths as  $g_c = 1.0$  and  $\epsilon = 0.5$  in Fig. 12f.

To reveal the long time behavior of the several collective dynamics, we plot the color coded Fig. 13 where x and y axes represent the systematic variation of coupling strength  $\mu$  and time, respectively. Figure 13a, b shows the time evolution of  $\mathbf{x}_1(n)$  and  $\mathbf{x}_2(n)$  with

**Fig. 13** The long time behavior of  $x_1(n)$  and  $x_2(n)$  is plotted against the systematic varied coupling strength  $\mu$  ( $= g_c = 2.0 \epsilon$ ) for various controlling parameters **a**, **b** for  $\alpha_1 = 3.9$ ,  $\alpha_2 = 4.1$ , and **c**, **d** for  $\alpha_1 = 2.1$ ,  $\alpha_2 = 4.8$ . The color bar stands for time evolution of  $x_1(n)$  and  $x_2(n)$  in **a**, **c** and **b**, **d**, respectively. (Color figure online)



respect to the coupling strength  $\mu$  for fixed values of the control parameters  $\alpha_1 = 3.9$  and  $\alpha_2 = 4.1$  at which the uncoupled neuron exhibits different dynamics such as chaotic square wave bursting ( $x_1(n)$ ) (firing) and steady state ( $x_2(n)$ ) (silence) (the corresponding time series are shown in Fig. 12a). For slight increment of coupling strength, the silence oscillators transit to oscillatory mode where as the firing one still oscillatory motion. Depending on the interaction strength  $\mu$ , the coupled systems produced desynchronized and synchronized behavior with different firing patterns and the associated time series are plotted in Fig. 12b, c. After the critical coupling strength  $\mu = 0.5$ , the coupled neuron oscillates in synchronized motion with small amplitude. Similarly, in the absence of coupling strengths, Fig. 13c, d represents the oscillatory and steady state for  $\alpha_1 = 2.1$ ,  $\alpha_2 = 4.8$  and after certain coupling value both the neuronal oscillators converge to different steady states. So, when the coupling is introduced between them, silence neuron will try to fire and the oscillatory neuron will fire in different patterns. Depending on the parameter mismatch, we get structurally different states for higher coupling strength. If the parameter mismatch between two neurons is small, and for higher coupling strengths, both will fire almost synchronously but higher parameter mismatch leads to suppression of oscillation.

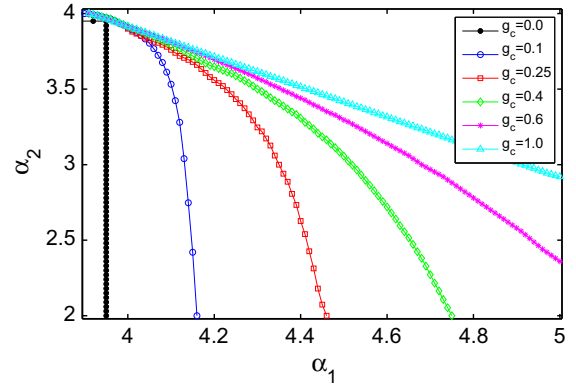


**Fig. 14** The steady state and oscillatory dynamics of coupled systems are plotted by taking the various values of the synaptic coupling strength  $g_c$  and  $\epsilon = \frac{g_c}{2}$  in the two control parameter space  $\alpha_1 - \alpha_2$

Further to reveal the firing and resting scenario of the coupled oscillators, we map the phase diagram (Fig. 14) of two control parameters  $\alpha_1$  and  $\alpha_2$  by considering the different values of the synaptic coupling strength  $g_c$  and  $\epsilon = \frac{g_c}{2}$ . The lower and upper regions of various color curves represent the steady state (silence) and oscillatory dynamics (firing), respectively, of the coupled systems. The black filled circle denotes the boundary curve for the transition from steady state to oscillatory state of two uncoupled ( $g_c = 0.0$ ,  $\epsilon = 0.0$ ) sys-

tems. The influences of the coupling strength are clearly shown in Fig. 14. The local dynamics of the isolated neuronal Rulkov model is steady state for  $0 < \alpha_1 = \alpha_2 < 4$  and oscillatory for  $\alpha_1 = \alpha_2 > 4$ . But introducing the interactions between the neurons, steady states converted to the oscillatory dynamics and vice versa.

## 7 Conclusions

In this paper, we systematically studied the collective behaviors of coupled Rulkov map based neuronal oscillators in the presence of both inner linking and chemical synaptic interactions. These type of interactions are more general to communicate between neurons. For such inter-neuronal communication, synchronization in neuronal networks is very crucial for normal and several cognitive functions [70], but may also reflect pathological brain states [71]. It has been shown that there are several factors such as coupling types [72] and strengths, noise [73] and existing cluster neural network which has strong influenced in the appearance burst synchronization in neuronal systems. Using the linear stability analysis, we derived the analytical condition for the stable steady state dynamics and oscillatory states of coupled systems. The master stability function approach is used to find the analytical condition for complete neuronal synchronization. We showed that increasing the value of synaptic coupling strength, enhancing of neuronal synchrony occurs, Fig. 5a, and variation of MSF in the parameter space  $\epsilon - g_c$  is shown in Fig. 5c. The global stability of the synchronization state is verified using basin stability measure (cf. Fig. 6).

During the transition among the several dynamical states, we have discussed the different types of bursting patters in the time evolution of each neuron (cf. Fig. 4). Next, we have investigated the time-delayed effect in the interaction function, and it has been shown that the presence of time delay in only the inner linking coupling induced the enhancement of neuronal synchrony. When time delay is introduced in the both couplings, we surprisingly observed that the enhancement of neuronal synchrony is possible up to a certain threshold of the delay time and further increased values of delay, and coupled neuronal systems show the de-enhancement, as shown in Fig. 7. Recently, it was shown that the synaptic interaction between the neurons may not occur continuously, and there may be a discontinuous connection

due to external noise or perturbation. In this context, stochastic blinking interaction between the neurons is very important from the neuroscience point of view. We studied the synchronization behavior of coupled systems in the presence of stochastic on-off interaction over time, and we found that as the probability of the off interaction increases, the critical coupling strength for synchronization gradually increases up to a certain threshold of that probability and beyond that no neuronal synchrony is possible, as shown in Fig. 8. Finally, we articulate the transition among different bursting and spiking dynamics of the coupled systems where primarily the uncoupled neurons are at steady state and oscillatory dynamics and after introducing the interaction between them, the each oscillator shows the different types of bursting and spiking patterns in desynchronization as well as synchronization motion depending upon the respective values of controlling and coupling strength, shown in Fig. 12. In order to recount the complexity of the interaction between the numerous number of neurons in a larger neural network, the neurons are often clotted and lumped within the synchronized subnetworks and such neuronal subpopulation comprised of both excitatory and inhibitory neurons which are spatially localized [74].

In realistic neuronal systems [75], a fraction of neurons are connected in a local area of the network via unfamiliar synapse, namely autapse. The autapse is associated with the self-feedback current on the membrane potential with memory and self-adjusting. So it is interesting to study the effect of autapse on neuronal synchrony in the coupled neuron. We showed that autaptic delay induced neuronal synchrony in the coupled neuron, as shown in Fig. 10. In this context, two mutually coupled neurons model may provide as a well illustration of two interacted neuronal sub-ensembles. Also, to conclude, we wish to point out that our findings may serve a good recipe to understand the several neuronal processes and coding information in many biological and physical aspects.

## Compliance with ethical standards

**Conflict of interest** The authors declare no conflict of interest.

## References

1. Azevedo, F.A.C., Carvalho, L.R.B., Grinberg, L.T., Farfel, J.M., Ferretti, R.E.L., Leite, R.E.P., Filho, W.J., Lent, R.,

- Herculano-Houzel, S.: Equal numbers of neuronal and non-neuronal cells make the human brain an isometrically scaled-up primate brain. *J. Comp. Neurol.* **513**, 532–541 (2009)
2. Pereda, A.E.: Electrical synapses and their functional interactions with chemical synapses. *Nat. Rev. Neurosci.* **15**, 250–263 (2014)
  3. Sun, H., Cao, H.: Complete synchronization of coupled Rulkov neuron networks. *Nonlinear Dyn.* **84**, 2423–2434 (2016)
  4. Singer, W.: Time as Coding Space in Neocortical Processing: A Hypothesis. Springer, Berlin (1994)
  5. Eckhorn, R.: Neural mechanisms of scene segmentation: recording from the visual cortex suggest basic circuits or linking field models. *IEEE Trans. Neural Netw.* **10**, 464–479 (1999)
  6. Singer, W., Gray, C.M.: Visual feature integration and the temporal correlation hypothesis. *Annu. Rev. Neurosci.* **18**, 555–586 (1995)
  7. Llinas, R., Ribary, U.: Coherent 40-Hz oscillation characterized dream state in humans. *Proc. Natl. Acad. Sci. USA* **90**, 2078–2081 (1993)
  8. Hartline, D.K.: Pattern generation in the lobster (panulirus) stomatogastric ganglion: pyloric network simulation. *Biol. Cybern.* **33**, 223–236 (1979)
  9. Bartsch, R., Kantelhardt, J.W., Penzel, T., Havlin, S.: Experimental evidence for phase synchronization transitions in the human cardiorespiratory system. *Phys. Rev. Lett.* **98**, 54102 (2007)
  10. Uhlhaas, P.J., Singer, W.: Neural synchrony in brain disorders: relevance for cognitive dysfunctions and pathophysiology. *Neuron* **52**, 155–168 (2006)
  11. Kandel, E.R., Schwartz, J.H., Jessell, T.M.: Principles of Neural Science. McGraw-Hill, New York (2000)
  12. Wang, Q.Y., Chen, G.R., Perc, M.: Synchronous bursts on scale-free neuronal networks with attractive and repulsive coupling. *PLoS ONE* **6**, e15851 (2011)
  13. Vida, I., Bartos, M., Jonas, P.: Shunting inhibition improves robustness of gamma oscillations in hippocampal interneuron networks by homogenizing firing rates. *Neuron* **49**, 107–177 (2006)
  14. Mao, X., Wang, Z.: Stability, bifurcation, and synchronization of delay-coupled ring neural networks. *Nonlinear Dyn.* **84**, 1063–1078 (2016)
  15. Balasubramaniam, P., Vembarasan, V.: Synchronization of recurrent neural networks with mixed time-delays via output coupling with delayed feedback. *Nonlinear Dyn.* **70**, 677–691 (2012)
  16. Xu, Y., Jia, Y., Ma, J., Hayat, T., Alsaedi, A.: Collective responses in electrical activities of neurons under field coupling. *Nonlinear Dyn.* **8**, 1349 (2018)
  17. Song, Z., Xu, J.: Codimension-two bursting analysis in the delayed neural system with external stimulations. *Nonlinear Dyn.* **67**, 309–328 (2012)
  18. Song, Z., Xu, J.: Bursting near Bautin bifurcation in a neural network with delay coupling. *Int. J. Neur. Syst.* **19**, 359–373 (2009)
  19. Guo, Y.: Exponential stability analysis of traveling waves solutions for nonlinear delayed cellular neural networks. *Dynam. Syst.* **32**, 490 (2017)
  20. Zhang, X., Li, P.J., Wu, F.P., Wu, W.J., Jiang, M., Chen, L., Qi, G.X., Huang, H.B.: Transition from winnerless competition to synchronization in time-delayed neuronal motifs. *Europhys. Lett.* **97**, 58001 (2012)
  21. Kunec, S., Bose, A.: Role of synaptic delay in organizing the behavior of networks of self-inhibiting neurons. *Phys. Rev. E* **63**, 021908 (2001)
  22. Pérez, T., García, G.C., Eguíluz, V.M., Vicente, R., Pipa, G., Mirasso, C.: Effect of the topology and delayed interactions in neuronal networks synchronization. *PLoS ONE* **6**, e19900 (2011)
  23. Tang, G., Xu, K., Jiang, L.: Synchronization in a chaotic neural network with time delay depending on the spatial distance between neurons. *Phys. Rev. E* **84**, 046207 (2011)
  24. Wang, Q., Perc, M., Duan, Z., Chen, G.: Synchronization transitions on scale-free neuronal networks due to finite information transmission delays. *Phys. Rev. E* **80**, 026206 (2009)
  25. Haken, H.: Pattern recognition and synchronization in pulse-coupled neural networks. *Nonlinear Dyn.* **44**, 269–276 (2005)
  26. Bera, B.K., Ghosh, D., Lakshmanan, M.: Chimera states in bursting neurons. *Phys. Rev. E* **93**, 012205 (2016)
  27. Bera, B.K., Ghosh, D.: Chimera states in purely local delay-coupled oscillators. *Phys. Rev. E* **93**, 052223 (2016)
  28. Wang, G., Jin, W., Hu, C.: The complete synchronization of MorrisLecar neurons influenced by noise. *Nonlinear Dyn.* **73**, 1715–1719 (2013)
  29. Bera, B.K., Ghosh, D., Banerjee, T.: Imperfect traveling chimera states induced by local synaptic gradient coupling. *Phys. Rev. E* **94**, 012215 (2016)
  30. Majhi, S., Perc, M., Ghosh, D.: Chimera states in uncoupled neurons induced by a multilayer structure. *Sci. Rep.* **6**, 39033 (2016)
  31. Maksimenko, V.A., Makarov, V.V., Bera, B.K., Ghosh, D., Dana, S.K., Goremyko, M.V., Frolov, N.S., Koronovskii, A.A., Hramov, A.E.: Excitation and suppression of chimera states by multiplexing. *Phys. Rev. E* **94**, 052205 (2016)
  32. Kundu, S., Majhi, S., Bera, B.K., Ghosh, D., Lakshmanan, M.: Chimera states in two-dimensional networks of locally coupled oscillators. *Phys. Rev. E* **97**, 022201 (2018)
  33. Zhou, J., Wu, Q., Xiang, L.: Impulsive pinning complex dynamical networks and applications to firing neuronal synchronization. *Nonlinear Dyn.* **69**, 1393–1403 (2012)
  34. Wang, C., Cao, H.: Stability and chaos of Rulkov map-based neuron network with electrical synapse. *Commun. Nonlinear Sci. Numer. Simulat.* **20**, 536–545 (2015)
  35. Hu, D., Cao, H.: Stability and synchronization of coupled Rulkov map-based neurons with chemical synapses. *Commun. Nonlinear Sci. Numer. Simulat.* **35**, 105–122 (2016)
  36. Guo, Y.: Globally robust stability analysis for stochastic COHEN-GROSSBERG neural networks with impulse control and time-varying delays. *Ukr. Math. J.* **69**, 1220–133 (2018)
  37. Aton, S.J., Herzog, E.D.: Come together, rightnow: synchronization of rhythms in a mammalian circadian clock. *Neuron* **48**, 531–534 (2005)
  38. Bredesen, D.E., Rao, R.V., Mehelen, P.: Cell death in the nervous system. *Nature* **443**, 796–802 (2006)
  39. Van Der Loos, H., Glaser, E.M.: Autapses in neocortex cerebri: synapses between a pyramidal cells axon and its own dendrites. *Brain Res* **48**, 355–360 (1972)

40. Lübke, J., Markram, H., Frotscher, M., Sakmann, B.: Frequency and dendritic distribution of autapses established by layer 5 pyramidal neurons in the developing rat neocortex: comparison with synaptic innervation of adjacent neurons of the same class. *J. Neurosci.* **16**, 3209–3218 (1996)
41. Ma, J., Song, X., Jin, W., Wang, C.: Autapse-induced synchronization in a coupled neuronal network. *Chaos Solitons Fractals* **80**, 31–38 (2015)
42. Ma, J., Song, X., Tang, J., Wang, C.: Wave emitting and propagation induced by autapse in a forward feedback neuronal network. *Neurocomputing* **167**, 378–389 (2015)
43. Wang, C., Ma, J.: A review and guidance for pattern selection in spatiotemporal system. *Int. J. Mod. Phys. B* **32**, 1830003 (2018)
44. Pecora, L.M., Carroll, L.T.: Master stability functions for synchronized coupled systems. *Phys. Rev. Lett.* **80**, 2109–2112 (1998)
45. Menck, P.J., Heitzig, J., Marwan, N., Kurths, J.: How basin stability complements the linear-stability paradigm. *Nat. Phys.* **9**, 89–92 (2013)
46. Rakshit, S., Bera, B.K., Majhi, S., Hens, C., Ghosh, D.: Basin stability measure of different steady states in coupled oscillators. *Sci. Rep.* **7**, 45909 (2017)
47. Rakshit, S., Majhi, S., Bera, B.K., Sinha, S., Ghosh, D.: Time-varying multiplex network: intralayer and interlayer synchronization. *Phys. Rev. E* **96**, 062308 (2017)
48. Rakshit, S., Bera, B.K., Perc, M., Ghosh, D.: Basin stability for chimera states. *Sci. Rep.* **7**, 2412 (2017)
49. Rulkov, N.F.: Regularization of synchronized chaotic bursts. *Phys. Rev. Lett.* **86**, 183 (2001)
50. Franović, I., Miljković, V.: The effects of synaptic time delay on motifs of chemically coupled Rulkov model neurons. *Commun. Nonlinear Sci. Numer. Simulat.* **16**, 623–633 (2011)
51. Genio, C.I.D., Gómez-Gardeñes, J., Bonamassa, I., Boccaletti, S.: Synchronization in networks with multiple interaction layers. *Sci. Adv.* **2**, e1601679 (2016)
52. Banerjee, R., Ghosh, D., Padmanaban, E., Ramaswamy, R., Pecora, L.M., Dana, S.K.: Enhancing synchrony in chaotic oscillators by dynamic relaying. *Phys. Rev. E* **85**, 027201 (2012)
53. Banerjee, R., Bera, B.K., Ghosh, D., Dana, S.K.: Enhancing synchronization in chaotic oscillators by induced heterogeneity. *Eur. Phys. J. Special Top.* **226**, 1893–1902 (2017)
54. Newman, J.P., Butera, R.J.: Mechanism, dynamics, and biological existence of multistability in a large class of bursting neurons. *Chaos* **20**, 023118 (2010)
55. Angeli, D., Ferrell Jr., J.E., Sontag, E.D.: Detection of multistability, bifurcations, and hysteresis in a large class of biological positive-feedback systems. *Proc. Natl. Acad. Sci. USA* **101**, 1822–1827 (2004)
56. Canavier, C.C., Baxter, D.A., Clark, J.W., Byrne, J.H.: Multiple modes of activity in a model neuron suggest a novel mechanism for the effects of neuromodulators. *J. Neurophys.* **72**, 872–882 (1994)
57. Kim, S., Park, S.H., Ryu, C.S.: Multistability in coupled oscillator systems with time delay. *Phys. Rev. Lett.* **79**, 2911 (1997)
58. Song, Z., Yang, K., Xu, J., Wei, Y.: Multiple pitchfork bifurcations and multiperiodicity coexistences in a delay-coupled neural oscillator system with inhibitory-to-inhibitory connection. *Commun. Nonlinear Sci. Numer. Simulat.* **29**, 327–345 (2015)
59. Park, S.H., Kim, S., Pyo, H.B., Lee, S.: Multistability analysis of phase locking patterns in an excitatory coupled neural system. *Phys. Rev. E* **60**, 2177 (1999)
60. Song, Z., Wang, C., Zhen, B.: Codimension-two bifurcation and multistability coexistence in an inertial two-neuron system with multiple delays. *Nonlinear Dyn.* **85**, 2099–2113 (2016)
61. Song, Z., Xu, J., Zhen, B.: Multitype activity coexistence in an inertial two-neuron system with multiple delays. *Int. J. Bifurc. Chaos* **25**, 1530040 (2015)
62. Song, Z., Xu, J., Zhen, B.: Stability switches and double Hopf bifurcation in a two-neural network system with multiple delays. *Cogn. Neurodyn.* **7**, 505–521 (2013)
63. Liu, J., Zhao, Z.: Multiple solutions for impulsive problems with non-autonomous perturbations. *App. Math. Lett.* **64**, 143–149 (2017)
64. Belykh, I.V., Belykh, V.N., Hasler, M.: Blinking model and synchronization in small-world networks with a time-varying coupling. *Physica D* **195**, 188 (2004)
65. Karabelas, A.B., Purrura, D.P.: Evidence for autapses in the substantia nigra. *Brain Res.* **200**, 467–473 (1980)
66. Preston, R., Bishop, G., Kitai, S.T.: Medium spiny neuron projection from the rat striatum: an intracellular horseradish peroxidase study. *Brain Res.* **183**, 253–263 (1980)
67. Park, M.R., Lighthall, J.W., Kitai, S.T.: Recurrent inhibition in the rat neostriatum. *Brain Res.* **194**, 359–369 (1980)
68. Guo, D., Wu, S., Chen, M., Perc, M., Zhang, Y., Ma, J., Cui, Y., Xu, P., Xia, Y., Yao, D.: Regulation of irregular neuronal firing by autaptic transmission. *Sci. Rep.* **6**, 26096 (2016)
69. Yilmaz, E., Ozer, M., Baysal, V., Perc, M.: Autapse-induced multiple coherence resonance in single neurons and neuronal networks. *Sci. Rep.* **6**, 30914 (2016)
70. Benedek, M., Bergner, S., Könen, T., Fink, A., Neubauer, A.C.: EEG alpha synchronization is related to top-down processing in convergent and divergent thinking. *Neuropsychologia* **49**, 3505–3511 (2011)
71. Traub, R.D., Wong, R.K.: Cellular mechanism of neuronal synchronization in epilepsy. *Science* **216**, 745–747 (1982)
72. Belykh, I., Lange, E., Hasler, M.: Synchronization of bursting neurons: what matters in the network topology. *Phys. Rev. Lett.* **94**, 188101 (2005)
73. Burić, N., Todorović, K., Vasović, N.: Influence of noise on dynamics of coupled bursters. *Phys. Rev. E* **75**, 067204 (2007)
74. Wilson, H.R., Cowan, J.D.: Excitatory and inhibitory interactions in localized populations of model neurons. *Biophys. J.* **12**, 1–24 (1972)
75. Ma, J., Tang, J.: A review for dynamics in neuron and neuronal network. *Nonlinear Dyn.* **89**, 1569–1578 (2017)